Submitted to Physical Review D

LBL-1537
Preprint

c.1

For Reference
Not to be taken from this room

A STUDY OF $K^+\pi^-$ SCATTERING IN THE REACTION $K^+p \to K^+\pi^-\Delta^{++}$ AT 12 GeV/c

M.J. Matison, A. Barbaro-Galtieri, M. Alston-Garnjost,
S.M. Flatte, J.H. Friedman, G.R. Lynch, M.S. Rabin,
and F.T. Solmitz

July 1973

Prepared for the U.S. Atomic Energy Commission
under Contract W-7405-ENG-48

LAWRENCE BERKELEY LABORATORY
UNIVERSITY OF CALIFORNIA
BERKELEY

DISCLAIMER

This document was prepared as an account of work sponsored by the United States Government. While this document is believed to contain correct information, neither the United States Government nor any agency thereof, nor the Regents of the University of California, nor any of their employees, makes any warranty, express or implied, or assumes any legal responsibility for the accuracy, completeness, or usefulness of any information, apparatus, product, or process disclosed, or represents that its use would not infringe privately owned rights. Reference herein to any specific commercial product, process, or service by its trade name, trademark, manufacturer, or otherwise, does not necessarily constitute or imply its endorsement, recommendation, or favoring by the United States Government or any agency thereof, or the Regents of the University of California. The views and opinions of authors expressed herein do not necessarily state or reflect those of the United States Government or any agency thereof or the Regents of the University of California.

A STUDY OF $K^+\pi^-$ SCATTERING IN THE REACTION $K^+p \rightarrow K^+\pi^-\Delta^{++}$ AT 12 GeV/c*

M. J. Matison, A. Barbaro-Galtieri, M. Alston-Garnjost, S. M. Flatté,[†] J. H. Friedman,[‡] G. R. Lynch, M. S. Rabin,[§] and F. T. Solmitz

Lawrence Berkeley Laboratory
University of California
Berkeley, California 94720

July 1973

ABSTRACT

We have studied $K^+\pi^-$ elastic scattering in the reaction $K^+p \rightarrow K^+\pi^-\Delta^{++}$ at 12 GeV/c, and in the $K\pi$ mass interval 800 to 1000 MeV. We have performed a partial wave analysis in this $K\pi$ mass region, dominated by the p-wave resonance $K^*(890)$, in order to obtain information about the s-wave amplitude. We have extrapolated the $K^+\pi^-$ moments, total cross section, and p-wave cross section to the pion pole. The p-wave cross section is close to the unitarity limit and can be described by a Breit-Wigner with parameters $M = 896 \pm 2$ MeV and $\Gamma = 47 \pm 3$ MeV. We then perform an energy-independent phase shift analysis of the extrapolated moments and total cross section using this Breit-Wigner for the p-wave and a previously determined small negative phase shift for the $I = 3/2$ s-wave. For the $I = 1/2$ s-wave phase shift we find the so called "down" solution, which has a phase-shift that rises slowly from 20° at $M(K\pi) = 800$ MeV to 60° at $M(K\pi) = 1000$ MeV. The energy dependence of this phase shift is well described by an effective range form with a scattering length $a_0^1 = -0.33 \pm 0.05$ F. The so-called "up" solution is eliminated or has large chi-squared everywhere except for two overlapping mass intervals at $M(K\pi) = 890$ and 900 MeV. However, due to limited statistics, we expect two solutions for the s-wave very near

the mass where the p-wave is resonant. We then perform an energy-dependent partial wave analysis and find again no evidence for an s-wave resonance although, due to limited statistics, we could not exclude one at 890 MeV with $\Gamma < 7$ MeV.

I. INTRODUCTION

Much work has been done in recent years in understanding $\pi\pi$[1] and $K\pi$[2-7] interactions. Since π and K mesons are not stable, their interactions must be studied indirectly, in reactions where the one-pion exchange mechanism is dominant. The I = 0 s-wave in $\pi\pi$ scattering and the I = 1/2 s-wave in $K\pi$ scattering have shown similar behavior in the mass regions near the ρ and the $K^*(890)$ respectively. Phase shift analyses have found two solutions: one called the "down" solution, and another sharply rising near the p-wave resonance, called the "up" solution. The "up" solution corresponds to a narrow s-wave resonance. Recently the "up" solution has been ruled out in $\pi\pi$ scattering.[8]

The analysis of $K^+\pi^-$ scattering with the largest number of events was done by Bingham et al.[5] They used 31 122 events of the reaction $K^+p \to K^+\pi^-\Delta^{++}$ and 4855 events of the reaction $K^+p \to K^0\pi^0\Delta^{++}$, with beam momenta from 2.5 to 12.7 GeV/c (compiled in the so-called World Data Summary Tape, WDST),[9] and found two solutions for the s-wave I-spin 1/2 phase shift (δ_0^1): a slowly increasing δ_0^1 which approaches about 70° at $M(K\pi)$ = 1.1 GeV and another rapidly rising ("up") solution which has a relatively narrow ($\leq$ 30 MeV) resonant state near 890 MeV.

The analyses of Trippe et al.[3] and Mercer et al.[4] (who used an earlier WDST compilation[9]) were done on the same reactions used by Bingham et al.,[5] but with smaller statistics, and did not find the "up" solution. The analyses of Firestone et al.[6] and Yuta et al.[7] were done on reactions of the type $KN \to NK\pi$ and found both the "up" and "down" solution. Recently Chung et al.[10] used a different method of analysis involving the study of angular distributions in the physical region, instead of data extrapolated to the pion pole as for previous analyses,[2-6] and found that the data can accommodate little, if any, narrow-width

s-wave state in the $K^*(890)$ region.

In this paper we study $K^+\pi^-$ elastic scattering in 11 073 events of the reaction $K^+p \to K^+\pi^-\Delta^{++}$ at 12 GeV/c. The experiment was done at SLAC using an rf-separated 12-GeV/c K^+ beam[11] and the 82-inch hydrogen bubble chamber. Six hundred thousand pictures were taken corresponding to a pathlength of 34.9 ± 1.0 events/μb.[12] The analysis is done by extrapolating angular distributions and cross sections to the pion pole. It differs from previous analyses in three respects: (a) it has larger statistics, except for Ref. 5, which had similar statistics for $P_K > 8$ GeV/c; (b) it has higher incident energy, which provides data at smaller momentum transfer, that is, closer to the pion pole; (c) it has data at only one energy and in one bubble chamber, making possible the use of absolute normalization to calculate cross sections. The use of cross sections is the main difference between our analysis and the one of Bingham et al.[5]

Section II contains a study of the reaction: the data are found to be consistent with the assumption that the reaction is dominated by one-pion exchange. Section III deals with extrapolation to the pion pole. We find that the extrapolated angular distribution at the π^+p vertex agrees with on-shell π^+p scattering for π^+p masses below 1.4 GeV. At the $K^+\pi^-$ vertex we extrapolate to the pion pole the moments of the $K^+\pi^-$ angular distribution, the total cross section, and the p-wave cross section. The p-wave cross section can be described by a Breit-Wigner with M = 896 ± 2 MeV and Γ = 47 ± 3 MeV. We use these parameters in the subsequent phase shift analysis.

In Sec. IV we discuss $K^+\pi^-$ scattering, first checking the agreement with unitarity of the extrapolated and unextrapolated moments. Next, an energy-independent phase shift analysis is done using only

the extrapolated moments in order to compare with the results of Bingham et al. We find both the "up" and "down" solutions. We then discuss the origin of the ambiguity. In order to resolve the ambiguity we perform another phase shift analysis including the extrapolated total cross section. We find only the down solution at all but two overlapping $K\pi$ mass intervals at $M(K\pi) = 890$ and 900 MeV. We then perform an energy-dependent partial wave analysis in order to find an upper limit for the width of a narrow s-wave resonance which could be compatible with our data. Finally, Sec. V contains a summary and conclusions.

II. THE DATA

A. Data Reduction

The reaction being studied, $K^+p \to K^+\pi^-\pi^+p$, is observed in the four-prong topology of which we have 189 000 examples. All of the film was scanned at least twice and 10% of the film was scanned a third time, giving an overall scanning efficiency close to 1.[13] The events were measured on the Spiral Reader. All failing events were remeasured, and half of the twice-failing events were measured a third time. The overall four-prong measuring efficiency is 0.897 ± 0.013.[14] Of these four-prongs, 30 163 have a best fit to the required reaction, but many of them are ambiguous with other four-constraint fits.[13] However, in the kinematic region of interest in this paper the ambiguities are less than 1% because both the π^+ and proton are slow in the laboratory and can be recognized from the ionization measurements made by the Spiral Reader.

B. The Reaction $K^+p \to K^+\pi^-\pi^+p$

The main features of this reaction can be seen in Figs. 1 through 4. The $K^+\pi^-$ mass spectrum (Fig. 1a) is dominated by the $K^*(890)$. There is also a strong $K^*(1420)$ signal. The $K^+\pi^-$ mass spectrum for events where the π^+p mass is in the Δ^{++} region [1.16 GeV $< M(\pi^+p) < 1.36$ GeV] is shown in Fig. 1b. The π^+p mass distributions for all events and for events with $M(K\pi) = 0.8$ to 1.0 GeV are shown in Figs. 1c and 1d; they are both dominated by the $\Delta^{++}(1236)$. The triangle plot, $M(K^+\pi^-)$ versus $M(\pi^+p)$, is shown in Fig. 2.

Some distributions of the four-momentum transfer squared between the proton and the π^+p system (t_{p,π^+p} and $t' = t - t_{min}$) are shown in Fig. 3. Figures 3a and 3d contain all events and Figs. 3b and 3e contain only $K^*(890)\,\Delta^{++}$ events, where the K^* is defined by $0.840 < M(K^+\pi^-) < 0.940$ GeV. Figure 3c shows the t distribution for the events used in the partial wave analysis, and Fig. 3f shows the t' distribution for K^* events. The distribution of $t_{p\Delta}$ (which we will refer to below as t) is sharply peaked at small $|t|$ with two-thirds of the data having $|t| < 0.1$ GeV^2. The minimum $|t|$ attained in this reaction in the $K^*(890)$ region is ≈ 0.015 GeV^2. The Chew-Low plot, t versus $M^2(K^+\pi^-)$, is shown in Fig. 4, for both the entire sample (Fig. 4a) and the subsample of events containing a Δ^{++} (Fig. 4b).

C. Test of One-Pion Exchange

The contribution of one-pion exchange to the reaction $K^+p \to \Delta^{++}K^+\pi^-$ has been discussed at great length by previous authors.[15] We study the range of validity of the one-pion exchange mechanism in our data by examining the K^* and Δ decay angles. The coordinate system used is defined in Fig. 5. We examine first the $K^*(890)$ region.

(1) Distribution in Treiman-Yang angles, $\phi_{K\pi}$ and $\phi_{\pi p}$. For one-pion exchange we expect the distribution of the Treiman-Yang angle to be isotropic in both the K^* and Δ^{++} rest frames. Figure 6 shows the $\phi_{K\pi}$ distributions for several intervals of t. For $|t| < 0.1$ GeV^2 the distribution is isotropic and for $|t| > 0.1$ GeV^2 it is somewhat less isotropic. Figure 7 shows these distributions for $\phi_{\pi p}$ in different intervals of t: we observe behavior similar to that of $\phi_{K\pi}$.

(2) Distribution in $\theta_{\pi p}$. If one-pion exchange dominates this reaction, we expect the moments of the π^+p angular distribution, $\langle Y_\ell^0 \rangle$, to approximate those calculated from real π^+p scattering experiments. Figure 8 shows the π^+p moments, $\ell = 1$ through 4, as a function of πp for $|t'| < 0.1$ GeV^2. The curves are the on-shell values.[16] The agreement in the Δ^{++} region is quite good, but for $M(\pi p) > 1.4$ GeV the data points are systematically higher than the on-shell curves.

(3) Distribution in $\theta_{K\pi}$. For formation of a p-wave state, $K^*(890)$, one-pion exchange predicts this distribution to be proportional to $\cos^2\theta_{K\pi}$. Figure 9 shows $\cos\theta_{K\pi}$ distributions for various t intervals. For $|t| < 0.2$ GeV^2 the distribution is approximately $\cos^2\theta$, with some asymmetry and a small constant component which, as we shall see in Sec. IV, can be adequately explained by the presence of a $K\pi$ s-wave.

For $K\pi$ masses above the $K^*(890)$ and below 1.2 GeV, we examine the same distributions (not shown) and find consistency with a dominant one-pion exchange mechanism: (1) the distributions in $\phi_{K\pi}$ and $\phi_{\pi p}$ are isotropic for small values of t and t' respectively, and (2) the moments of the π^+p angular distributions are very close to those calculated from real π^+p scattering for small $|t'|$ and $M(\pi^+p) < 1.4$ GeV.

In summary we find that one-pion exchange can describe the data when the π^+p mass is in the Δ^{++} region, the $K\pi$ mass is below 1.2 GeV, and $|t|$ is small. For large values of $|t|$ there are departures from pure one-pion exchange, which may be due to other exchanges or absorption. For π^+p masses above the Δ^{++} there are large discrepancies between the πp moments and real πp scattering. This point will be discussed in Sec. III. A. 1.

III. EXTRAPOLATION TO THE PION POLE

We have established that the data are consistent with one-pion exchange in the Δ^{++} region and for small $|t|$. We will now extrapolate the moments of the angular distribution and the cross section from the physical region ($|t| > t_{min}$) to the pion pole ($t = m_\pi^2 \equiv \mu^2 = 0.019$ GeV^2) where the values should be equal to on-shell scattering. We expect the one-pion exchange contribution to dominate over any background near the pion pole. In practice, however, the values obtained from the extrapolation may have an error greater than the statistical error, because the form of the extrapolation may not be correct.

A. Moment Extrapolations

If we expand the differential cross-section in the form

$$\frac{d\sigma}{d\Omega} = \frac{\sigma}{\sqrt{4\pi}\, a_0} \sum_{\ell=0}^{\ell_{max}} a_\ell Y_\ell^0 (\cos\theta)$$

then the expansion coefficients a_ℓ are proportional to the "moments," i.e., the expectation values of the spherical harmonics

$$\langle Y_\ell^0 \rangle = \frac{a_\ell}{\sqrt{4\pi}\, a_0}$$

To calculate the ℓth moment for the N events in given intervals of $K^+\pi^-$ mass, π^+p mass, and t, we estimate the expectation value, $\langle Y_\ell^0 \rangle$, by its sample mean, and calculate the error $\Delta \langle Y_\ell^0 \rangle$ using the relations

$$\langle Y_\ell^0 \rangle = \frac{1}{N} \sum_{i=1}^{N} Y_\ell^0(\cos\theta_i)$$

$$\Delta \langle Y_\ell^0 \rangle = \left[\frac{\langle (Y_\ell^0)^2 \rangle - \langle Y_\ell^0 \rangle^2}{N} \right]^{\frac{1}{2}} .$$

In order to obtain the value of the ℓth "moment," $\langle Y_\ell^0 \rangle_{ext}$, at the pion pole for a particular $K\pi$ and πp mass interval we fit a linear dependence on $|t|$ to the experimental moments in the physical region and then calculate the value and error at $t = \mu^2$.

1. π^+p Moments

In order to check the extrapolation precedure we first study the π^+p moments, since the on-shell moments for π^+p scattering have been measured. We extrapolate to the pion pole, using only those events where the $K^+\pi^-$ mass is in the region of the K^*. The results of the linear extrapolation are shown in Table I and Fig. 8. The chi-squared (χ^2) per degree of freedom (N_D), reported in Table I, show that linear extrapolation is satisfactory for our data. The extrapolated values, just as in the case of the small $|t'|$ data, agree with on-shell scattering for $M(\pi p) < 1.4$ GeV. For $M(\pi p) > 1.4$ GeV the extrapolated moments show no improvement over the moments with $|t'| < 0.1$ GeV^2.

The discrepancies in the moments at high πp mass could be explained as reflections of the Q bump, a threshold enhancement in the $K\pi\pi$ system.[17,18] Similar discrepancies have been observed in other reactions,[1] e.g., $\pi^+p \to \pi^+\pi^-\pi^+p$ and $pp \to \pi^-p\pi^+p$, and could similarly be explained by the reflections of the A1, a $\rho\pi$ threshold enhancement in the $\pi\pi\pi$ system which, like the Q, is related to a diffraction phenomena. The Dalitz plots for the final-state $K^*(890)\,\pi^+p$ for all events and for some t' cuts are shown in Fig. 10. The Q enhancement can be clearly seen at all values of t' and all values of πp mass; however, it is relatively less important for small πp masses, especially in the Δ^{++}

band. It is plausible that the discrepancies in the high πp mass are due to the Q because:

(1) The Q is prominent at higher πp masses.

(2) Q events populate the small-angle scattering in the πp angular distribution, making all the moments more positive.

(3) The Q is still present at small values of $|t'|$, so it might affect the extrapolated values.

These points can be checked in a reaction where there are no strong diffraction phenomena, for example, the reaction $pp \to p\pi^+n$. In this case the agreement between the high-mass π^+p moments and the on-shell moments is very good.[19]

For the $K\pi$ moments the analogous problem would be with the $\Delta^{++}\pi$ threshold enhancement. The Dalitz plots for the final-state $K^+\pi^-\Delta^{++}$ for all the events and some t' cuts are shown in Fig. 11. Although the $\Delta^{++}\pi^-$ enhancement is less dominant than the Q, we might expect that the $K\pi$ moments at high $K\pi$ masses would be somewhat too positive. However, the $\Delta^{++}\pi$ enhancement is relatively less important for low $K\pi$ mass and small $|t'|$, so we do not expect distortion of the lower mass $K\pi$ moments.

In summary, we find that we can reproduce the π^+p on-shell moments in the Δ^{++} region either by using a small $|t'|$ average or a simple extrapolation. It is reasonable to assume that similar methods will approximate on-shell results at the $K\pi$ vertex in the $K^*(890)$ mass region. However, for $K\pi$ masses much larger than 890 MeV, one might expect, in analogy with the π^+p system, that the extrapolated moments are poor estimates of the on-shell moments.

2. $K^+\pi^-$ Moments

We will be considering in detail the $K\pi$ mass region $0.80 < M(K\pi) < 100$ GeV, where there are 3267 events. The $K\pi$ angular distribution in this mass region for $|t| < 0.1$ GeV^2 is shown in Fig. 12. Figure 13 shows the first four moments of the angular distribution, $\langle Y_1^0 \rangle$ through $\langle Y_4^0 \rangle$, plotted versus $K\pi$ mass up to 2 GeV. In calculating these moments we have used events with a Δ^{++} and with $|t'| < 0.1$ GeV^2. Near the $K^*(890)$ $\langle Y_2^0 \rangle$ is ≈ 0.2, which indicates a large amount of p-wave, since we expect $\langle Y_2^0 \rangle = 0.252$ for pure p-wave. The moment $\langle Y_1^0 \rangle$, which is large below the $K^*(890)$, measures the s-p interference. The $\langle Y_3^0 \rangle$ and $\langle Y_4^0 \rangle$ moments are consistent with zero for $K\pi$ masses less than 1.2 GeV, which indicates that waves higher than p are not observed in the data at these masses.

Since at the πp vertex in the Δ^{++} region, both the $|t'| < 0.1$ GeV^2 and the extrapolated moments are a good approximation to the on-shell πp scattering, we try using both sets of data at the $K\pi$ vertex. We use overlapping $K\pi$ mass bins, 20 MeV wide, whose centers are separated by 10 MeV. This choice allows a direct comparison with previous analyses. However, it should be kept in mind that only one-half of the points are statistically independent. For the extrapolation we use data up to values of $|t| = 0.3$ or 0.4 GeV^2, depending on the $K\pi$ mass bin; this $|t|$ interval includes about 95% of the events. We find that linear extrapolations give reasonable χ^2's (average $\chi^2/N_D = 1.1$, where N_D is the number of degrees of freedom). The linear extrapolations for $\langle Y_1^0 \rangle$ and $\langle Y_2^0 \rangle$ are shown in Figs. 14 and 15, and the results are summarized in Table II. The extrapolated moments versus $K\pi$ mass are shown in Fig. 16 and the unextrapolated moments with $|t'| < 0.1$ GeV^2 (hereafter called the small $|t|$ moments) in Fig. 17. The extrapolated

and small $|t|$ moments have similar mass dependence, but the extrapolated moments are systematically higher.

We also perform a quadratic extrapolation and find that the χ^2's per degree of freedom do not improve (average $\chi^2/N_D = 1.2$). The quadratic extrapolations are summarized in Table III.

B. Cross-Section Extrapolation

The extrapolation of the total cross section to the pion pole is more elaborate than the extrapolation of normalized moments since the cross section has a rapid t dependence. Wolf[20] has studied the t dependence of the differential cross section ($d\sigma/dt$) for the reaction $\pi^+p \to \Delta^{++}\rho$ at various incident momenta and found that $d\sigma/dt$ was adequately described by the one-pion exchange formalism modified by Dürr and Pilkuhn form factors[21] and by a slowly varying factor G(t). This DP-OPE model for $d\sigma/dt$ has been successfully used for many reactions[15] and finally applied to extrapolations to the pion pole by Ma et al.[22] They studied the reaction $pp \to \Delta^{++}n$ and found that a conventional Chew-Low extrapolation procedure[23] did not reproduce satisfactorly the known on-shell π^+p cross section in the Δ^{++} region, whereas the introduction of DP form factors and Wolf's G(t) factor gave very good agreement. This procedure has since been used by many authors,[1-6, 8] and we use it to extrapolate our data.

1. Total Cross Section

In the case of one-pion exchange, the differential cross section, modified by Dürr-Pilkuhn and Wolf form factors, is

$$\frac{d^3\sigma}{dmdMdt} = \frac{1}{4\pi^3 m_p^2 P_L^2} \frac{m^2 q(m)\sigma(m)\ M^2 Q(M)\sigma(M)}{(t-\mu^2)^2} F(m,M,t), \qquad (1)$$

where $F(m,M,t)$ is a form factor which is 1 at the pion pole and has

the form

$$F(m,M,t) = (DP)_{\pi p \text{ vertex}} \times (DP)_{K\pi \text{ vertex}} \times G^2(t) \qquad (2)$$

with $(DP)_{K\pi} = 1$ for s-wave,

$$(DP)_{K\pi} = \left[\frac{q_t(m,t)}{q\ (m)}\right]^2 \frac{1 + R^2_{K^*} q^2(m)}{1 + R^2_{K^*} q_t^2(m,t)} \quad \text{for p-wave,}$$

$$(DP)_{\pi p} = \frac{(M+m_p)^2 - t}{(M+m_p)^2 - \mu^2} \left[\frac{Q_t(M,t)}{Q\ (M)}\right]^2 \frac{1 + R^2_\Delta Q^2(M)}{1 + R^2_\Delta Q_t^2(M,t)}, \qquad (3)$$

$$G(t) = \frac{c - \mu^2}{c - t}.$$

Here the symbol DP has been used for the Dürr and Pilkhun form factors and G(t) for the slowly varying additional factor introduced by Wolf.[20] The remaining symbols used in Eqs. (1)-(3) are as follows:

m_p = proton mass

P_L = lab beam momentum

$\sigma(m) = K^+\pi^-$ cross section

$\sigma(M) = \pi^+ p$ cross section

$m = M(K^+\pi^-)$

$M = M(\pi^+ p)$

μ = pion mass

$q(m)$ = outgoing K^+ momentum in the $K^+\pi^-$ c. m.

$Q(M)$ = outgoing proton momentum in the $\pi^+ p$ c. m.

$q_t(m,t)$ = virtual π momentum in the $K^+\pi^-$ c. m.

$Q_t(M,t)$ = virtual π momentum in the $\pi^+ p$ c. m.

The values of the numerical constants were taken to be:

$$R_\Delta = 3.97 \pm 0.11 \text{ GeV}^{-1},$$
$$R_{K^*} = 1.25 \pm 0.20 \text{ GeV}^{-1},$$
$$c = 2.29 \pm 0.27 \text{ GeV}^2.$$

R_Δ and c were obtained by Wolf,[20] who fitted many reactions over a large energy range. The value R_{K^*} has been obtained by Trippe et al.[3]

by fitting data of the reactions $K^+p \to \Delta^{++}K^*$ and $K^-p \to K^{*0}n$ at various momenta between 3 and 14 GeV/c.[15]

For each $K\pi$ mass interval and t interval we define a quantity

$$"\sigma_{m,t}" = \frac{\left(\frac{d\sigma}{dt}\right)_{\text{experimental}}}{\left(\frac{d\sigma}{dt}\right)_{\text{DP-OPE}}}, \qquad (4)$$

where $\left(\frac{d\sigma}{dt}\right)_{\text{DP - OPE}}$ stands for the integration of the right-hand side of Eq. (1) over the Δ^{++} mass region and over a $K\pi$ mass interval and t interval:

$$\left(\frac{d\sigma}{dt}\right)_{\text{DP-OPE}} = \frac{1}{4\pi^3 m_p^2 P_L^2} \int dM \int dm \int dt \ \frac{m^2 q(m)\, M^2 Q(M)\, \sigma(M)}{(t-\mu^2)^2} \times F(m,M,t),$$

with $\sigma(M)$ taken to be the on-shell π^+p cross section, and $\sigma(m)$ set equal to 1. For each $K\pi$ mass interval we calculate $"\sigma_{m,t}"$ for several t intervals, fit a straight line through these points (Fig. 18), and calculate a value of the cross section at $t = \mu^2$. This value, σ_T, should be the on-shell $K\pi$ cross section averaged over the mass interval under consideration, assuming that there are no rapid variations within the interval.

These results are shown in Fig. 19 and Table IV. The peak at a mass of about 895 MeV exceeds the p-wave unitarity limit, which is consistent with the presence of some s-wave.

2. P-Wave Cross Section

Since there is no indication of d-wave in our data at these $K\pi$ masses (Sec. III. A. 2), we can write the total cross section and moments in terms of only s and p waves as follows:

$$\sigma_T = 4\pi \lambda^2 \left(|s|^2 + 3\,|p|^2 \right) = \sigma_s + \sigma_p ,$$

$$\langle Y_1^0 \rangle = \sqrt{\frac{3}{\pi}}\, \frac{\mathrm{Re}\,(sp^*)}{|s|^2 + 3\,|p|^2} = \sqrt{\frac{3}{\pi}}\, \frac{|s|\,|p|\,\cos \Phi_{sp}}{|s|^2 + 3\,|p|^2} , \qquad (5)$$

$$\langle Y_2^0 \rangle = \frac{3}{\sqrt{5\pi}}\, \frac{|p|^2}{|s|^2 + 3\,|p|^2} .$$

The p-wave cross section is then

$$\sigma_p = \sqrt{5\pi}\, \langle Y_2^0 \rangle\, \sigma_T .$$

We can extrapolate this expression to the pion pole and isolate σ_p, which allows us to obtain the best p-wave parameters that describe our data for use in the subsequent partial wave analysis. This also gives us the opportunity to check independently the validity of the extrapolation procedure.

To obtain σ_p we multiply "$\sigma_{m,t}$", defined in Eq. (4), in every t and m interval by $\sqrt{5\pi}\ \langle Y_2^0 \rangle$ and then make a linear extrapolation of "σ_p" to the pion pole. The results are shown in Fig. 20 and Table V. The maximum value of σ_p is in agreement with the unitarity limit for the I = 1/2 p-wave $[p = (2/3)p_{1/2}]$, and this gives us confidence in the extrapolation. The values of σ_p are fitted by a Breit-Wigner resonance with the form[24]

$$\sigma_p = 16\pi\, \lambda^2 \sin^2 \delta_1^1 \qquad (6)$$

with $\cot \delta_1^1 = \dfrac{m_R - m}{\Gamma/2}$,

where $\Gamma = \Gamma_R \dfrac{2m_R}{m_R + m} \dfrac{q^3(m)}{q_R^3} \dfrac{1 + R^2 q_R^2}{1 + R^2 q^2(m)}$

where m_R and Γ_R are the mass and width of the resonance, respectively, and R = 2 fermi.

We obtain the parameters

$$m_R = 896 \pm 2 \text{ MeV},$$
$$\Gamma_R = 47 \pm 3 \text{ MeV},$$

with $\chi^2 = 5.5$ for 6 degrees of freedom. These fitted values are consistent with the average value quoted by the Particle Data Group for neutral K^*, $M_R = 896.7 \pm 0.7$ MeV, and $\Gamma_R = 51.7 \pm 1.0$ MeV.[25]

IV. PARTIAL WAVE ANALYSIS

The $K\pi$ s-wave can be easily studied in the $K^*(890)$ region; in fact $K^*(890)$ is a p-wave resonance with well-known behavior which can be used to study the s-wave through the s-p interference term. As already noted, we see no evidence for the presence of d-wave for $M(K\pi) < 1.20$ GeV. The phase shift analysis, therefore, will only involve s and p waves. The relations among the extrapolated quantities $\langle Y_1^0 \rangle$, $\langle Y_2^0 \rangle$, σ_T and the s and p amplitudes have already been given in Eq. (5), Sec. III. B. 2.

We will confine the partial wave analysis to $M(K\pi) < 1.0$ GeV, because the extrapolation to the pion pole is more reliable at low $K\pi$ masses, as discussed in Sec. III. A. 1, and also because at these low masses all the amplitudes can be assumed to be elastic. This last point has been discussed in the review of Trippe.[2] In our data we find a total of 34 events for $M(K\pi\pi) < 1.0$ GeV in the reactions $K^+p \to \Delta^{++}K^{\pm}\pi^{\pm}\pi^{0}$ for all $|t|$ values, to be compared with 3436 events in the reaction $K^+p \to \Delta^{++}K^+\pi^-$ with $M(K^+\pi^-) < 1.0$ GeV and the same $|t|$ values; we therefore can safely assume the inelasticity to be zero.

A. Partial Wave Amplitudes

The partial wave amplitudes for $K^+\pi^-$ scattering can have two I-spin components, I = 1/2 and I = 3/2. The I-spin composition is as follows:

$$s = \frac{2}{3} s_{1/2} + \frac{1}{3} s_{3/2} , \tag{7}$$

$$p = \frac{2}{3} p_{1/2} + \frac{1}{3} p_{3/2} .$$

In terms of the phase shifts, δ_ℓ^{2I}, the partial waves are:

$$s_I = e^{i\delta_0^{2I}} \sin \delta_0^{2I} ,$$

$$p_I = e^{i\delta_1^{2I}} \sin \delta_1^{2I} . \tag{8}$$

There are four parameters in these amplitudes, two I = 3/2 and two I = 1/2 phase shifts.

The I = 3/2 amplitudes have been studied in $K^+\pi^+$ and $K^-\pi^-$ interactions by various authors[26] and reviewed by Trippe.[2] Two groups have attempted to extract phase shifts for the s and p waves and found the $p_{3/2}$ to be very small or consistent with zero, for $M(K\pi) < 1.0$ GeV. For the s-wave the two analyses are consistent with an I = 3/2 s-wave parametrization of the form

$$\sigma_0^3 = \frac{4\pi}{q^2} \sin^2 \delta_0^3 = 1.8 \text{ mb}. \tag{9}$$

We use this form, which has already been used by Bingham et al.,[5] with a negative sign for δ_0^3 as determined in experiments that used both $K^+\pi^-$ and $K^0\pi^0$ data.[4,5]

For the I = $\frac{1}{2}$ amplitudes we have already shown in Sec. III.B that the p-wave in our data can adequately be described by a Breit-Wigner amplitude for a K^* resonance with m = 896 MeV and Γ = 47 MeV. This implies that our data do not show any need for a $p_{3/2}$ partial wave, in agreement with the results from $K^-\pi^-$ and $K^+\pi^+$ data.[2,26] Since we use the BW parameterization [Eq. (6)] for the p-wave, we are left with only one partial wave, $s_{1/2} = e^{i\delta_0^1} \sin \delta_0^1$, to determine.

B. Calculation of the Phase and Magnitude of s separately: Check of Unitarity

For real $K^+\pi^-$ scattering we expect the phase and magnitude of an amplitude to be related by Eq. (8), which constrains the amplitude to lie on the unitary circle in an Argand plot.

In order to check if the data satisfy unitarity we can use two measured quantities, $\langle Y_1^0 \rangle$ and $\langle Y_2^0 \rangle$, to determine the phase and magnitude of $s_{1/2}$, using Eqs. (5)-(9) and setting $p_{3/2} = 0$. Figure 21 shows $s_{1/2}$ calculated in this way for several $K\pi$ masses. The results from the extrapolated moments are shown on the left, those from small $|t|$ moments on the right. As expected there are two s-wave solutions at each $K\pi$ mass except where $\phi_{sp} = 0$ (in the first mass intervals for extrapolated moments), since only the absolute value of the s-p phase difference, ϕ_{sp}, is determined.

The amplitudes calculated from the extrapolated moments satisfy unitarity reasonably well, while the ones from the small t data give a magnitude for $s_{1/2}$ which is too large. This shows that the small $|t|$ data do not obey unitarity and that they are likely to be less representative of on-shell $K\pi$ scattering. This may be due, for example, to some constant background in the $K\pi$ angular distribution which could increase the magnitude of $s_{1/2}$.

C. Fit of δ_0^1 to $\langle Y_1^0 \rangle$ and $\langle Y_2^0 \rangle$

We now do an overconstrained fit for δ_0^1, using the extrapolated $\langle Y_1^0 \rangle$ and $\langle Y_2^0 \rangle$ and using eq. (8) for the $s_{1/2}$ amplitude, therefore imposing unitarity. From Eqs. (7) and (8) we obtain:

$$|s|^2 = \frac{1}{9}\left[4\sin^2\delta_0^1 + \sin^2\delta_0^3 + 4\sin\delta_0^1\sin\delta_0^3\cos(\delta_0^1-\delta_0^3)\right],$$

$$|p|^2 = \frac{4}{9}\sin^2\delta_1^1, \tag{10}$$

$$\mathrm{Re}(sp^*) = \frac{2}{9}\sin\delta_1^1\left[2\sin\delta_0^1\cos(\delta_0^1-\delta_1^1) + \sin\delta_0^3\cos(\delta_0^3-\delta_1^1)\right].$$

Here δ_0^3 is given by Eq. (9), the p-wave by Eq. (6) as previously discussed, therefore δ_0^1 is the only free parameter. From these equations and Eq. (5) we calculate $\langle Y_1^0(\delta_0^1)\rangle$ and $\langle Y_2^0(\delta_0^1)\rangle$. Then, for each $K\pi$ mass bin, δ_0^1 is varied to minimize the χ^2.

$$\chi^2 = \sum_{\ell=1}^{2}\left[\frac{\langle Y_\ell^0(\delta_0^1)\rangle - \langle Y_\ell^0\rangle_{ext}}{\Delta\langle Y_\ell^0\rangle_{ext}}\right]^2,$$

where the subscript ext refers to the extrapolated values.

The results of this fit are shown in Fig. 22 and summarized in Table VI. Plots of χ^2 versus δ_0^1 for each $K\pi$ mass interval are shown in Fig. 23. There are two distinct solutions (i.e., χ^2 has two minima) at some $K\pi$ masses between $M(K\pi) = 860$ and 960 MeV, although Table VI shows that the "up" solution is never missing in two adjacent mass intervals. There is only one solution below $M(K\pi) = 860$ MeV, and above 960 MeV (not shown). Figure 22 is a plot of the values of δ_0^1 corresponding to the χ^2 minima. It shows a slowly varying "down" solution, which (see Table VI) fits the moments with an average χ^2 of 1.5 per degree of freedom. Starting at 860 MeV one could also draw a rapidly rising "up" solution which has no point at 870 MeV, a point with large χ^2 at 880 MeV, and above 960 MeV can be continued through the "down + 180° solution." Therefore, there seems to be a twofold ambiguity for the s-wave phase shift, although the "up" solution has large χ^2 at one point, no solution at all at another, and lacks smoothness. In the next section we will discuss the nature of this ambiguity.

D. Discussion of the "Up-Down" Ambiguity

The discussion which follows will show that the ambiguity observed is characterized by two factors:

(a) Information on the size of the s-wave amplitude is crucial in solving the ambiguity. In fact if the moments $\langle Y_1^0\rangle$ and $\langle Y_2^0\rangle$ used in the previous section had very small errors and if the $I = 3/2$ s-wave were zero, by knowing the size of the amplitude we would expect an ambiguous solution only at the mass of $K^*(890)$.

(b) The $K^*(890)$ plays an important role in the ambiguity. If an s-wave resonance like solution really exists, it has to be at a mass very close to 890 MeV, in order to produce a slowly varying smooth solution like the "down" solution.

To illustrate point (a) we will assume that δ_0^1 is given by a straight line (s_1 in Fig. 24) similar to the "down" solution, and then calculate $\langle Y_1^0\rangle_c$ and $\langle Y_2^0\rangle_c$ using Eqs. (5)-(8) and assuming $s_{3/2} = p_{3/2} = 0$. We now take the ratio of the $\langle Y_1^0\rangle_c$ and $\langle Y_2^0\rangle_c$, thus discarding information on the magnitude of $|s|$. Multiplying this ratio by $|p|$, we get $|p|\langle Y_1^0\rangle_c / \langle Y_2^0\rangle_c = |s|\cos\phi_{sp}$; this quantity is clearly the projection of the s-wave on the p-wave (Fig. 25). If we now recalculate δ_0^1 we find two solutions, s_1 and s_2, at every $K\pi$ mass; that is, we get both the slowly varying "down" solution that we started with and a sharply rising "up" solution (Fig. 24). In Sec. IV-C we used $\langle Y_1^0\rangle$ and $\langle Y_2^0\rangle$ separately, and this provided enough information to eliminate the "up" solution for $M(K\pi) < 860$ MeV and $M(K\pi) > 960$ MeV (Fig. 22) but not enough information to eliminate it completely between 860 and 960 MeV. By using σ_T in the fit we should be able to add further information on the magnitude of the s-wave and be able to narrow down the mass region of the ambiguity; this fit will be discussed in the next section.

However, even if σ_T is used in the limit in which $s_{3/2} = 0$ (Fig. 25), both magnitudes and both projections of $s_{1/2}$ on the p-wave would be the same at M = 896 MeV; therefore, the ambiguity could not be resolved at this mass. For a small $s_{3/2}$ and limited statistics we still expect an ambiguity near the $K^*(890)$ mass.

To illustrate point (b) we will assume that the s-wave is a resonance with a certain mass M_s and Γ_s = 50 MeV; we then calculate $\langle Y_1 \rangle_c$ and $\langle Y_2 \rangle_c$, take their ratio as before and again calculate δ_0^1. Figure 26 shows the two solutions obtained for various values of M_s. Figure 26c shows the case in which the input "up" solution has M = 880 MeV, which gives an acceptable "down" solution. However when we start with resonances with M = 840 or 860 or 900 or 920 MeV (Figs. 26a, b, d, e respectively) the "down" solution no longer has smooth behavior, and at some $K\pi$ mass is "unphysical." In fact, in each case for some $K\pi$ masses the phase shift decreases at a rate that violates Wigner's causality condition.[27] In other words, if a resonant solution is the real one, the resonance occurs in a narrow mass region near the $K^*(890)$, where we will get two physically acceptable solutions.

E. Energy-Independent Fit Using $\langle Y_1^0 \rangle$, $\langle Y_2^0 \rangle$, and σ_T

As discussed in the previous section we need as much information as possible on the magnitude of the s-wave amplitude in order to resolve the up-down ambiguity. Therefore we do a fit using $\langle Y_1^0 \rangle$, $\langle Y_2^0 \rangle$, and σ_T as input. The results are shown in Figs. 27 and 28 and Table VII.

Figure 27 shows plots of χ^2 versus δ_0^1 for the fits in each mass interval. For the "down" solution the average χ^2 is 2.0 for two degrees of freedom. The "up" solution follows an interesting pattern. For masses much below the $K^*(890)$ the second solution is absent. It begins to appear with a slight asymmetry in the χ^2 plot at 870 MeV, and

at 880 MeV where there is a shoulder with a very large χ^2. At 890 and 900 MeV the solutions are equally good. At 910 MeV, the second solution is already beginning to have a large χ^2, and at 920 MeV the χ^2 becomes unacceptable.

Figure 28 shows the plot of the values of δ_0^1 corresponding to all the χ^2 minima obtained in the fits, including the points with large χ^2, shown in parentheses. Figure 29 shows a comparison of the quantities $\langle Y_1^0 \rangle$, $\langle Y_2^0 \rangle$, and σ_T with the result of the fits; the "up" solution is shown also for the points which give large χ^2, and it is easily seen that the major contribution to the large χ^2 comes from the total cross section. Figure 28 shows that the "up" solution is reduced to only two overlapping points at 890 and at 900 MeV, as expected for the previously discussed ambiguity at the $K^*(890)$ mass. To obtain a continuous solution with these two points one has to draw a curve which connects them with the "down" solution below 890 MeV and with a "down + 180°" solution above 900 MeV.

We have investigated the dependence of these results on the parameters used for the $K^*(890)$ by altering the mass and width of the resonance. Figure 30 shows the results of a fit using $\langle Y_1^0 \rangle$, $\langle Y_2^0 \rangle$, and σ_T, and a p-wave Breit-Wigner with M = 900 MeV and Γ = 50 MeV (respectively two and one standard deviations from the fitted values discussed in Sec. III. B. 2). Although the χ^2 for some of the points of the "up" solution has improved, we still find that only two overlapping points in the up solution could meaningfully be connected to the down solution below 890 MeV and the "down + 180°" solution above 900 MeV.

We now discuss the two solutions separately.

1. The "Down" Solution

The phase shifts of the down solution have a smooth and slowly

varying behavior and therefore can be parametrized by an effective-range formula:

$$k \cot \delta_0^1 = - \frac{1}{a_0^1} + \frac{1}{2} r_0^1 k^2, \tag{11}$$

where k is the K^+ momentum in the $K^+\pi^-$ center of mass, a_0^1 is the scattering length, and r_0^1 is the effective range. We have done a fit to alternate values of δ_0^1 from Table VII and found

$$a_0^1 = - 0.31 \pm 0.05 \text{ F}, \tag{12}$$

$$r_0^1 = - 1.4 \pm 0.5 \text{ F}.$$

We used only every other entry starting at 810 MeV, since the mass bins overlap. Figure 31 shows the fitted curve to this set of δ_0^1. The fit is reasonably good, the chi-square being 10.6 for 8 degrees of freedom. The phase shift rises from 20° to 60° between 810 and 990 MeV and, if it were to follow the energy dependence of this fit, it would cross 90° at M = 1114 MeV.

We have searched the complex energy plane for poles of the T matrix

$$T = \frac{1}{\cot \delta - i}$$

and found a pole in sheet II, defined according to the convention of Frazer and Hendry,[28] at M = 1062 MeV and $\Gamma/2$ = 234 MeV, which corresponds to the crossing of 90° in the physical region. However, since we are not using any values of δ_0^1 above 990 MeV this result is not conclusive.

Griffith[29] has used current algebra techniques to estimate the s-wave $K\pi$ scattering lengths. The results are

$$a_0^1 = 2 \frac{m_K}{m_K + m_\pi} \frac{m_\pi}{4\pi f^2} \quad \text{and} \quad a_1^3 = \frac{1}{2} a_0^1,$$

where $f = f_\pi$ is a coupling constant. Taking for f the value $f = 126 \pm 6$ MeV from the compilation of Ebel et al.,[30] we find the predicted values to be

$$(a_0^1) = - 0.22 \pm 0.02 \text{ F}, \qquad (a_0^3) = 0.11 \pm 0.01 \text{ F},$$

in agreement with our experimental value $a_0^1 = - 0.31 \pm 0.05$ F from Eq. (12) and the value $a_0^3 = 0.12$ F obtained by using Eqs. (9) and (11).

2. The "up" Solution

The up solution is obtained only at two overlapping points, at 890 and 900 MeV. As already discussed in Sec. IV.D we expect at this mass a phase ambiguity intrinsic to the analysis. In addition the distributions of $\langle Y_1^0 \rangle$, $\langle Y_2^0 \rangle$, and σ_T as a function of $K\pi$ mass do not show any sharp variations, which in general are associated with a narrow resonance. Therefore, there is no evidence in our data for an up resonant solution. However, one can still draw a continuous up solution by connecting the two points at 890 and 900 MeV with the down solution below 890 MeV and the "down + 180°" solution above 900 MeV. This would correspond to a very narrow s-wave resonance at this mass. The resolution of this experiment at the $K^*(890)$ mass is $\Gamma/2$ = 5 MeV;[31] however, we have chosen to analyze the data in 20-MeV intervals in order to have sufficient statistical accuracy for the extrapolation. In order to investigate for what width an s-wave resonance is incompatible with our data, we perform next an energy-dependent analysis.

F. Energy-Dependent Partial Wave Analysis

We parametrize the $s_{1/2}$ amplitude as

$$s_{1/2} = \frac{1}{\cot \delta_0^1 - i}. \tag{13}$$

Since the amplitude is elastic, a simple way to combine a background and resonant amplitude preserving unitarity is to add the two phase

shifts as follows:[32]

$$\delta_0^1 = \delta_B + \delta_R , \tag{14}$$

where δ_B is given by Eq. (11), which fits the "down" solution very well, and δ_R is the phase of an s-wave resonance of the form

$$\cot\delta_R = \frac{M_s - m}{\Gamma/2} ,$$
$$\Gamma = \Gamma_s \frac{2 M_s}{M_s + m} \frac{q}{q_s} . \tag{15}$$

Here M_s and Γ_s are the mass and width of the resonance, m is the $K\pi$ mass, and q_s is the momentum of the $K\pi$ system at the mass M_s.

If we include a resonance, the s-wave amplitude has four parameters: a_0^1, r_0^1, M_s, and Γ_s. We have 28 data points as input, $\langle Y_1^0 \rangle$, $\langle Y_2^0 \rangle$ and σ_T at 10 different non-overlapping $K\pi$ mass values, which we use for an overall fit (the total cross sections were not extrapolated at the lowest and highest mass). Since the data points are average values over 20-MeV mass intervals, we calculate an average of the function over 20-MeV bins and in addition we fold in the mass resolution as a Gaussian with a ± 5-MeV width at half maximum.[31] For each data point we calculate in this way the expected value of the function and then calculate a chi-square. We minimize the sum of the χ^2 over the 28 data points to find values of the parameters.

We find that the non-resonant hypothesis, that is $\delta_R = 0$ in Eq. (14), fits as well as the resonant hypothesis. However, the width of the resonance for the best resonant fit is $\Gamma_s < 1$ MeV, which we cannot detect since we have 20-MeV bins and ± 5 MeV resolution. At two standard deviations from the best resonant fit the width is $\Gamma_s = 7$ MeV. The data used in the fit are shown in Fig. 32, where the solid curve represents the scattering length fit, $\delta_R = 0$ in Eq. (14), and the dashed curve

represents the fit for $\Gamma_s = 7$ MeV. A resonance with this width could produce a detectable effect especially in the Y_1^0 and σ_T distributions. The non-resonant fit gives $a_0^1 = -0.33$, $r_0^1 = -1.1$, $\chi^2 = 36.0$ for 26 degrees of freedom, with parameters in agreement with the ones obtained in the energy-independent fit [Eq. (12)].

V. SUMMARY AND CONCLUSION

We have done an energy-independent phase shift analysis of $K^+\pi^-$ elastic scattering in the reaction $K^+p \to K^+\pi^-\Delta^{++}$ at 12 GeV/c, for $K\pi$ masses between 800 and 1000 MeV. First we fitted δ_0^1 to the extrapolated moments only. We find a slowly varying "down" solution which is approximately a straight line varying from 20° at $M(K\pi) = 800$ MeV to 60° at $M(K\pi) = 1000$ MeV. At some $K\pi$ masses we found a second solution with acceptable χ^2. This second solution, when connected to the lower branch of the down solution and the upper branch of the "down + 180°" solution, could give a resonant-like "up" solution, although the "down" solution would be favored over such an "up" solution on the basis of χ^2.

(a) If the "down" solution is the true solution (there is no narrow resonance), then, due to the mathematical ambiguity discussed in Sec. IV.D, there will always be an "up" solution near the $K^*(890)$, i.e., the "down" solution together with the rapidly changing p-wave of the K^* gives rise to a spurious "up" solution.

(b) If the "up" solution is the true solution (there is a narrow resonance), then the "up" solution together with the $K^*(890)$ p-wave will give rise to a "down" solution. However, this "down" solution will not have reasonable smooth behavior unless such a resonance has a mass close to 890 MeV. In other words, if the "up" solution corresponds to a resonance, it occurs

at just the mass that would allow the spurious "down" solution to also have reasonable behavior.

We then made a fit for δ_0^1 using the extrapolated moments and total cross section and find that the points of the "up" solution on either side of the $K^*(890)$ are eliminated or have large χ^2. The remaining points at the overlapping energies $M(K\pi) = 890$ and 900 MeV are at a mass where the ambiguity cannot be resolved with the present accuracy of the data. One can still draw a continuous solution by connecting these two points with the "down" solution below 890 MeV and the "down $+180°$" solution above 900 MeV, which would correspond to a narrow resonance added to a smooth background. However, there is no evidence for a narrow resonance in the distributions of $\langle Y_1 \rangle$, $\langle Y_2 \rangle$, and σ_T, which exhibit a smooth behavior.

In order to investigate how narrow a resonance can be compatible with our data we have done an energy-dependent partial wave analysis. We have used in the fit extrapolated values of $\langle Y_1 \rangle$, $\langle Y_2 \rangle$, and σ_T and parametrized the s-wave with a resonance added to an effec-range form for the background. We again find no evidence for a resonance, although since we have limited statistics and a mass resolution of ± 5 MeV we cannot exclude an $s_{1/2}$ resonance with $\Gamma < 7$ MeV.

The analysis of Bingham et al.,[5] who used the WDST compilation data,[9] found two solutions that fitted the data equally well: a "down" solution similar to ours and an "up" solution corresponding to a resonance added to background with $\Gamma < 30$ MeV. In our experiment we have better mass resolution, and in addition we have included the total cross-section measurements in the fit, thus adding constraints in the fit. We find no "up" solution, but due to limited statistics could not include one corresponding to a resonance with $\Gamma_s < 7$ MeV. The other analyses

discussed in Sec. I which found two solutions had fewer statistics than our analysis. Chung et al., who used a different method of analysis, agree with our conclusions.[10]

In conclusion, we find that the s-wave $K\pi$ scattering in the 0.8- to 1.0-GeV mass region is adequately represented by a phase shift slowly varying from 20° to 60°. Its energy dependence is well represented by an effective range formula with a scattering length $a_0^1 = -0.31 \pm 0.05$ F and an effective range $r_0^1 = -1.4 \pm 0.5$ F. The scattering length is in agreement with the current algebra calculation of Griffith:[29] $a_0^1 = -0.22 \pm 0.02$ F.

Footnotes and References

*Work done under the auspices of the U. S. Atomic Energy Commission.

†Present address: University of California-Santa Cruz, Santa Cruz, California.

‡Present address: Stanford Linear Accelerator Center, Stanford, California.

§Present address: University of Massachusetts, Amherst, Massachusetts.

1. See, for example, P. E. Schlein, Review of Some Experimental Results on the $\pi\pi$ and $K\pi$ Interactions, in Proceedings of the International School of Subnuclear Physics, Erice (1970).

2. For a recent review see T. G. Trippe, Recent Experimental Studies of the $K\pi$ Interactions, in Zero Gradient Synchrotron Workshops, Summer 1971, ANL/HEP 7208, Vol. I, p. 6 (1971).

3. T. G. Trippe et al., Phys. Letters 28B, 143 (1968).

4. R. Mercer et al., Nucl. Phys. B32, 381 (1971).

5. H. H. Bingham et al., Nucl. Phys. B41, 1 (1972).

6. A. Firestone et al., Phys. Rev. Letters 26, 1460 (1971).

7. H. Yuta et al., Phys. Rev. Letters 26, 1502 (1971).

8. S. D. Protopopescu et al., A $\pi\pi$ Phase Shift Analysis from Reactions $\pi^+p \to \pi^+\pi^-\Delta^{++}$ and $\pi^+p \to K^+K^+K^-\Delta^{++}$ at 7.1 GeV/c, in Experimental Meson Spectroscopy - 1972, edited by A. H. Rosenfeld and K. W. Lai (AIP, 1972), p. 17. See also S. D. Protopopescu et al., Phys. Rev. D 7, 1279 (1973).

9. The K^+p World Data Summary Tape contains events from 8 different experiments conducted at 11 laboratories in Europe and the USA. See Refs. 4 and 5 for more details.

10. S. U. Chung, R. L. Eisner, and M. Aguilar-Benitez, Phys. Rev. Letters 29, 1570 (1972).

11. S. Flatté, Manual for K82 Beam Watchers, LBL Group A Physics Note No. 646, Feb. 1968 (unpublished).

12. P. Davis and S. Flatté, K82 Path Length Determination, LBL Group A Physics Note No. 700, Jan. 1970 (unpublished).

13. For further discussion of this final state see P. J. Davis et al., Phys. Rev. D 5, 2688 (1972).

14. P. J. Davis and S. Flatté, K82 Measuring Efficiencies for Event Types 4 and 12, LBL Group A Physics Note No. 724, Feb. 1971 (unpublished).

15. P. E. Schlein, Meson Spectroscopy, p. 161, edited by C. Baltay and A. H. Rosenfeld (Benjamin, New York, 1968).

16. The moments were calculated from the phase shift analysis of A. Donnachie et al., Phys. Letters 26B, 161 (1968).

17. For discussion of the Q bump in our data see P. J. Davis et al., Ref. 13.

18. For a discussion of the effect of the Q bump on the π^+p moments see P. E. Schlein in Proceedings of the Conference on $\pi\pi$ and $K\pi$ Interactions (Argonne National Laboratory, 1969), p. 446.

19. E. Colton and P. Schlein, in Proceedings of the Conference on $\pi\pi$ and $K\pi$ Interactions (Argonne National Laboratory, 1969), p. 1.

20. G. Wolf, Phys. Rev. Letters 19, 925 (1967).

21. H. Dürr and H. Pilkuhn, Nuovo Cimento 40A, 899 (1965).

22. Z. Ming Ma et al., Phys. Rev. Letters 23, 342 (1969).

23. G. F. Chew and F. E Low, Phys. Rev. 113, 1640 (1959).

24. A. Barbaro-Galtieri, Baryon Resonances, in Advances in Particle Physics, Vol. 2, edited by R. L. Cool and R. E. Marshak (Wiley, New York, 1968), p. 197.

25. Particle Data Group, Review of Particle Properties, Rev. Mod. Phys. 45, S1 (1973).

26. For a complete list of references see T. G. Trippe, Ref. 2. Two of the experiments have attempted a phase shift analysis: A. M. Bakker et al., Nucl. Phys. B24, 211 (1970), and Meson Resonances and Related Electromagnetic Phenomena page 53, edited by R. H. Dalitz and A. Zichichi (International Physics Series, Bologna, 1971) p. 53; B. Jongejans and K. Voorthius, ibid., p. 57.

27. R. D. Tripp, Baryon Resonances, in Proceedings of the International School of Physics Enrico Fermi, Strong Interactions (Academic Press, New York, 1966), p. 70.

28. W. R. Frazer and A. W. Hendry, Phys. Rev. 134, B1307 (1964).

29. R. W. Griffith, Phys. Rev. 176, 1705 (1968).

30. G. Ebel et al., Nucl. Phys. B83, 317 (1971).

31. P. J. Davis et al., Phys. Rev. Letters 23, 1071 (1969).

32. See, for example, similar fits made for the $\Delta^{++}(1236)$ in A. Barbaro-Galtieri, "Selected Topics in Baryon Resonances," Lectures for the 1971 Erice Summer School, Lawrence Berkeley Laboratory Report LBL-555 (1972), to be published by Academic Press.

Table I. π^+p moments at the pion pole obtained by linear extrapolation. The reaction used is $K^+ + p \rightarrow K^* \pi^+ p$.

π^+p mass (GeV)	$\langle Y_2^0 \rangle$	$d\langle Y_1^0 \rangle$	χ^2/N_D	$\langle Y_1^0 \rangle$	$d\langle Y_2^0 \rangle$	χ^2/N_D
1.15-1.20	-0.100	0.021	0.8	0.068	0.021	0.8
1.20-1.23	-0.022	0.023	0.6	0.109	0.022	0.4
1.23-1.26	0.039	0.024	0.4	0.129	0.022	1.9
1.26-1.32	0.092	0.022	1.3	0.110	0.019	1.6
1.32-1.40	0.174	0.025	1.2	0.153	0.025	1.3
1.40-1.50	0.318	0.021	1.6	0.246	0.029	0.6
1.50-1.75	0.288	0.020	0.8	0.300	0.021	1.3
1.75-2.00	0.253	0.026	0.9	0.337	0.023	0.5
2.00-2.30	0.373	0.017	0.6	0.411	0.021	0.5

	$\langle Y_3^0 \rangle$	$d\langle Y_3^0 \rangle$		$\langle Y_4^0 \rangle$	$d\langle Y_4^0 \rangle$	
1.15-1.20	-0.048	0.021	0.6	0.008	0.021	0.7
1.20-1.23	-0.004	0.022	0.5	-0.003	0.022	0.5
1.23-1.26	-0.026	0.023	0.6	0.020	0.022	0.8
1.26-1.32	0.008	0.020	1.5	-0.052	0.019	0.9
1.32-1.40	-0.003	0.028	0.9	-0.044	0.028	1.1
1.40-1.50	0.122	0.033	1.1	0.059	0.034	0.9
1.50-1.75	0.174	0.027	1.3	0.094	0.028	0.5
1.75-2.00	0.303	0.029	0.8	0.268	0.029	1.5
2.00-2.30	0.435	0.025	0.9	0.376	0.031	1.3

Table II. $K^+\pi^-$ moments at the pion pole obtained by linear extrapolation. The reaction used was $K^+ + p \rightarrow \Delta^{++} K^+ \pi^-$.

$K\pi$ mass (GeV)	No. of events	$\langle Y_1^0 \rangle$	$d\langle Y_1^0 \rangle$	χ^2/N_D	$\langle Y_2^0 \rangle$	$d\langle Y_2^0 \rangle$	χ^2/N_D
0.810-0.830	96	0.350	0.040	0.4	0.153	0.056	0.3
0.820-0.840	104	0.343	0.045	1.0	0.210	0.057	0.9
0.830-0.850	152	0.248	0.040	0.7	0.218	0.042	1.8
0.840-0.860	190	0.261	0.036	2.4	0.174	0.036	1.3
0.850-0.870	293	0.204	0.029	1.1	0.161	0.027	0.9
0.860-0.880	430	0.230	0.026	1.8	0.211	0.022	0.9
0.870-0.890	576	0.193	0.023	0.5	0.229	0.019	0.3
0.880-0.900	732	0.122	0.021	0.4	0.210	0.018	0.5
0.890-0.910	719	0.079	0.022	0.7	0.206	0.017	0.7
0.900-0.920	594	0.067	0.024	0.9	0.207	0.019	1.4
0.910-0.930	456	0.075	0.027	1.0	0.188	0.022	0.8
0.920-0.940	324	0.030	0.032	0.6	0.215	0.026	1.4
0.930-0.950	266	-0.021	0.037	0.7	0.199	0.032	1.2
0.940-0.960	219	-0.050	0.042	1.6	0.224	0.034	1.8
0.950-0.970	172	0.009	0.055	0.2	0.192	0.047	0.4
0.960-0.980	166	-0.019	0.052	0.7	0.059	0.048	2.2
0.970-0.990	146	-0.035	0.060	3.6	0.086	0.058	1.0

Table III. $K^+\pi^-$ moments at the pion pole obtained by quadratic extrapolation.

Kπ mass (GeV)	$\langle Y_1^0 \rangle$	$d\langle Y_1^0 \rangle$	χ^2/N_D	$\langle Y_2^0 \rangle$	$d\langle Y_2^0 \rangle$	χ^2/N_D
0.810-0.830	0.35	0.11	0.7	0.08	0.15	0.3
0.820-0.840	0.37	0.13	2.0	0.29	0.17	1.7
0.830-0.850	0.33	0.10	0.7	0.36	0.10	1.6
0.840-0.860	0.30	0.07	3.5	0.26	0.08	1.4
0.850-0.870	0.14	0.06	1.0	0.19	0.06	1.1
0.860-0.880	0.11	0.06	0.3	0.23	0.05	1.1
0.870-0.890	0.17	0.05	0.5	0.23	0.04	0.5
0.880-0.900	0.10	0.04	0.4	0.20	0.04	0.6
0.890-0.910	0.08	0.04	0.9	0.20	0.03	0.8
0.900-0.920	0.05	0.05	1.0	0.15	0.04	1.2
0.910-0.930	0.07	0.06	1.2	0.14	0.05	0.7
0.920-0.940	0.03	0.07	0.7	0.17	0.05	1.4
0.930-0.950	-0.02	0.08	1.0	0.22	0.07	1.6
0.940-0.960	0.12	0.09	0.9	0.28	0.08	2.2
0.950-0.970	0.00	0.16	0.4	0.13	0.12	0.3
0.960-0.980	-0.09	0.15	1.0	0.20	0.14	3.4
0.970-0.990	-0.48	0.21	2.8	0.31	0.19	0.6

Table IV. $K^+\pi^-$ total cross section extrapolated to the pion pole.

$K\pi$ mass (GeV)	σ_T (mb)	χ^2/N_D
0.810-0.830	10.9±2.7	1.8
0.820-0.840	9.9±2.9	2.9
0.830-0.850	19.7±2.4	0.9
0.840-0.860	26.7±2.7	1.2
0.850-0.870	39.5±3.1	0.7
0.860-0.880	51.7±3.7	0.4
0.870-0.890	66.1±4.0	0.5
0.880-0.900	84.7±4.5	1.1
0.890-0.910	84.8±4.1	2.3
0.900-0.920	67.1±3.7	2.9
0.910-0.930	49.9±3.2	1.7
0.920-0.940	34.7±2.6	1.7
0.930-0.950	22.7±2.9	1.3
0.940-0.960	16.8±2.7	1.6
0.950-0.970	15.9±3.3	1.0
0.960-0.980	17.6±3.1	0.9

Table V. $K^+\pi^-$ p-wave cross section extrapolated to the pion pole.

Kπ mass (GeV)	σ_p (mb)	χ^2/N_D
0.810-0.830	6.3 ± 3.7	0.1
0.820-0.840	10.3 ± 4.0	0.3
0.830-0.850	13.9 ± 3.3	1.3
0.840-0.860	15.7 ± 3.3	1.2
0.850-0.870	21.6 ± 3.7	2.0
0.860-0.880	39.7 ± 4.8	1.9
0.870-0.890	56.5 ± 5.4	1.0
0.880-0.900	67.2 ± 6.0	0.6
0.890-0.910	64.1 ± 5.3	0.5
0.900-0.920	50.0 ± 4.7	2.0
0.910-0.930	34.5 ± 4.1	1.1
0.920-0.940	26.7 ± 3.4	0.6
0.930-0.950	19.3 ± 4.1	0.2
0.940-0.960	15.9 ± 3.8	0.4
0.950-0.970	12.8 ± 4.3	0.2
0.960-0.980	3.7 ± 4.0	2.0

Table VI. Values of the phase shift δ_0^1 obtained in the fit to extrapolated $\langle Y_1^0 \rangle$ and $\langle Y_2^0 \rangle$.

Kπ mass (GeV)	"Down" solution δ_0^1 (degrees)	χ^2 ($N_D = 1$)	"Up" solution δ_0^1 (degrees)	χ^2 ($N_D = 1$)
0.790-0.810	31 ± 8	0.9		
0.800-0.820	19^{+11}_{-4}	0.9		
0.810-0.830	25 ± 5	4.5		
0.820-0.840	26 ± 6	3.9		
0.830-0.850	23^{+6}_{-4}	0.6		
0.840-0.860	34^{+12}_{-8}	0.0		
0.850-0.870	34^{+44}_{-7}	2.9	64^{+10}_{-16}	1.9
0.860-0.880	37 ± 6	0.2		
0.870-0.890	37 ± 5	0.3	94^{+8}_{-12}	11.7
0.880-0.900	34 ± 5	1.6	130 ± 5	0.3
0.890-0.910	36 ± 5	2.2	153 ± 5	2.0
0.900-0.920	43 ± 5	0.1	167 ± 5	2.9
0.910-0.930	53 ± 6	0.1	170 ± 5	7.5
0.920-0.940	45 ± 8	3.3	183 ± 5	1.4
0.930-0.950	41^{+9}_{-12}	1.3	192^{+40}_{-6}	2.3
0.940-0.960	15^{+10}_{-5}	0.4		
0.950-0.970	53 ± 14	3.1	187 ± 6	1.5
0.960-0.980	59 ± 11	0.2		
0.970-0.990	56^{+14}_{-12}	0.0		
0.980-1.000	36^{+16}_{-25}	0.6		

Table VII. Values of the phase shift obtained in the fit to extrapolated $\langle Y_1^0 \rangle$, $\langle Y_2^0 \rangle$, and σ_T.

Kπ mass (GeV)	"Down" solution δ_0^1 (degrees)	χ^2 ($N_D = 2$)	"Up" solution δ_0^1 (degrees)	χ^2 ($N_D = 2$)
0.790-0.810	30 ± 7	1.0		
0.800-0.820	19^{+10}_{-4}	1.0		
0.810-0.830	24± 4	4.6		
0.820-0,840	23 ± 4	5.3		
0.830-0.850	29 ± 5	2.4		
0.840-0.860	37 ± 5	0.1		
0.850-0.870	48 ± 6	3.0		
0.860-0.880	43 ± 6	1.7		
0.870-0.890	38 ± 5	0.6	shoulder at 100	33.7
0.880-0.900	36 ± 4	2.7	133 ± 5	2.3
0.890-0.910	39 ± 5	3.7	151 ± 5	3.2
0.900-0.920	45 ± 4	0.9	163 ± 5	10.3
0.910-0.930	54 ± 5	0.1	164 ± 5	21.3
0.920-0.940	48 ± 5	3.6	179^{+7}_{-6}	21.8
0.930-0.950	40 ± 6	1.3		
0.940-0.960	31^{+8}_{-16}	2.4		
0.950-0.970	45 ± 8	3.5	187^{+8}_{-6}	6.6
0.960-0.980	56 ± 7	0.4		
0.970-0.990	58 ± 9	0.1		
0.980-1.000	56 ± 9	2.5		

Figure Captions

Fig. 1. (a) $K^+\pi$ mass distribution for all the events

(b) $K^+\pi^-$ mass distribution for Δ^{++} events [$1.16 < M(\pi^+p) < 1.36$ GeV]

(c) π^+p mass distribution for all the events

(d) π^+p mass distribution for the events used to study $K\pi$ scattering.

Fig. 2. Triangle plot of $M(K^+\pi^-)$ versus $M(\pi^+p)$, all events.

Fig. 3. Four-momentum transfer squared between the target and the outgoing π^+p system: (a) -t for all the events, (b) -t for $\Delta^{++}K^*$ events, (c) -t for $\Delta^{++}K^+\pi^-$ events for $M(K^+\pi^-) = 0.8$-1.0 GeV, (d) $-t'_{p,\pi^+p} = -t_{p,\pi^+p} + t_{min}$ for all the events, (e) -t' for $\Delta^{++}K^*$ events, (f) -t' for $p\pi^+K^*$ events.

Fig. 4. Chew-Low plot. (a) $M^2(K^+\pi^-)$ versus $-t_{p,\pi^+p}$ for all the events (24 266). (b) $M^2(K^+\pi^-)$ versus $-t_{p\Delta}$ for the Δ^{++} events (10 101).

Fig. 5. (a) One-pion exchange diagram, (b) t-channel coordinate system (Jackson frame) for the $K\pi$ vertex. $\phi_{K\pi}$ is the Treiman-Yang angle. An analogous frame can be defined for the πp system.

Fig. 6. Treiman and Yang angle $\phi_{K\pi}$ in the $K^+\pi^-$ center of mass for $K^+p \to \Delta^{++}K^*(890)$ events. (a) Events with $|t| < 0.1$ GeV^2 (1551), (b) events with $|t| = 0.1$ to 0.2 GeV^2 (460), (c) events with $|t| = 0.2$ to 0.3 GeV^2 (198), (d) events with $|t| = 0.3$ to 0.5 GeV^2 (156).

Fig. 7. Treiman and Yang angle for $\phi_{\pi p}$ in the π^+p center of mass for $K^+p \to \Delta^{++}K^*(890)$ events. (a)-(d) same t intervals as for Fig. 6.

Fig. 8. Extrapolated moments of the π^+p angular distribution versus π^+p mass for events of the reaction $K^+p \to \pi^+pK^*(890)$. The dots represent the unextrapolated values for $|t'| < 0.1$ GeV^2; the points at the lowest π^+p mass are the unextrapolated values since the statistics were not enough for an extrapolation.

Fig. 9. $K\pi$ scattering angle, $\cos\theta_{K\pi}$. $K^*(890)\,\Delta^{++}$ events. (a) - (d) same t intervals as for Fig. 6.

Fig. 10. Invariant mass squared of the $K^*(890)\,\pi$ system versus π^+p invariant mass squared.

Fig. 11. Invariant mass squared of the $\Delta^{++}\pi^-$ system versus the invariant mass squared of the $K^+\pi^-$ system.

Fig. 12. Angular distribution of the $K^+\pi^-$ scattering angle for the reaction $K^+p \to \Delta^{++}K^+\pi^-$ for $M(K^+\pi^-) = 0.8$ to 1.0 GeV and $|t| < 0.1\ \mathrm{GeV}^2$ (2038 events).

Fig. 13. $K^+\pi^-$ moments versus $K^+\pi^-$ mass for the events of the reaction $K^+p \to \Delta^{++}K^+\pi^-$ and with $|t'| < 0.1\ \mathrm{GeV}^2$.

Fig. 14. Extrapolation of the $K^+\pi^-$ moments to the pion pole. The $\langle Y_1^0 \rangle$ moment is shown versus $-t$ for different $K^+\pi^-$ mass intervals. The t bins are chosen for each $K^+\pi^-$ mass interval in such a way that each bin contains at least 25, and on the average 60, events.

Fig. 15. Extrapolation of the $\langle Y_2^0 \rangle$ moment; see the caption for Fig. 14.

Fig. 16. $K^+\pi^-$ extrapolated moments versus $K\pi$ mass. Values for overlapping $K\pi$ mass bins are shown.

Fig. 17. $K^+\pi^-$ moments with $|t| < 0.1\ \mathrm{GeV}^2$ (small $|t|$ moments) versus $K\pi$ mass. Values for overlapping $K\pi$ mass bins are shown.

Fig. 18. Extrapolation of "σ" to the pion pole, $t = \mu^2$, for different $K\pi$ mass intervals. The leftmost point, "σ" $(t = \mu^2)$, is assumed to be the $K^+\pi^-$ total cross section at the pion pole.

Fig. 19. Extrapolated $K^+\pi^-$ total cross section versus $K\pi$ mass. Values for overlapping $K\pi$ mass bins are shown. The curve is the p-wave unitarity limit.

Fig. 20. Extrapolated p-wave cross section versus $K\pi$ mass. The curve is a Breit-Wigner fitted to the data, $M = 896 \pm 2$ MeV and

$\Gamma = 47 \pm 3$ MeV. $\chi^2 = 5.5$ for 6 degrees of freedom.

Fig. 21. Argand plots for the $K\pi$ $I = 1/2$ s-wave. The phase and magnitude of $s_{1/2}$ are calculated from $\langle Y_1^0 \rangle$ and $\langle Y_2^0 \rangle$; unitarity is not imposed. Extrapolated data, left, and small $|t|$ data, right, for several $K\pi$ mass intervals. The p-wave is a Breit-Wigner and the $I = 3/2$ s-wave is given by Eq. (9).

Fig. 22. $I = 1/2$ s-wave phase shift from an energy-independent fit of δ_0^1 to $\langle Y_1^0 \rangle$ and $\langle Y_2^0 \rangle$. The p-wave is a Breit-Wigner with parameters determined from the data, $M = 896$ and $\Gamma = 47$ MeV, and δ_0^3 corresponds to Eq. (9). A solution with unacceptable χ^2 is plotted with parentheses and the χ^2 is given.

Fig. 23. χ^2 versus δ_0^1 for the fits of Fig. 22.

Fig. 24. Illustration of the "up-down" ambiguity. For each $K\pi$ mass, δ_0^1 is calculated from $\langle Y_1^0 \rangle / \langle Y_2^0 \rangle$ (which in turn has been calculated from s_1, a straight-line approximation to the "down" solution). At all $K\pi$ masses we obtain a new solution s_2 in addition to s_1. Information about the magnitude of $s_{1/2}$ is not used.

Fig. 25. Illustration of the "up-down" ambiguity. Calculation of δ_0^1 from $\langle Y_1^0 \rangle / \langle Y_2^0 \rangle$ giving two s-waves, $s_1 = s_{down}$ and $s_2 = s_{up}$. (a) $M(K\pi) = 870$ MeV, $|s_1| \neq |s_2|$; (b) $M(K\pi) = 890$ MeV. Here $|s_1| = |s_2|$ and the ambiguity cannot be resolved.

Fig. 26. Effects of varying the mass of a resonant "up" solution. Starting with s-wave resonances at various masses with $\Gamma_s = 50$ MeV, the ambiguous solutions are calculated using $\langle Y_1^0 \rangle / \langle Y_2^0 \rangle$. For $M_s = 880$ MeV, the two solutions approximate those of Fig. 22. For other values of M_s we no longer get a physically reasonable "down" solution.

Fig. 27. χ^2 versus δ_0^1 for the fit of δ_0^1 to $\langle Y_1^0 \rangle$, $\langle Y_2^0 \rangle$, and σ_T.

Fig. 28. s-wave phase shift, δ_0^1, from an energy-independent fit to the extrapolated $\langle Y_1^0 \rangle$, $\langle Y_2^0 \rangle$, and σ_T with p-wave parameters $M = 896$, $\Gamma = 47$ MeV. Solutions with large χ^2 are plotted with parentheses and the χ^2 is shown. Average χ^2 for the "down" solution is 2.0 for two degrees of freedom. Values for overlapping $K\pi$ mass bins are shown.

Fig. 29. Comparison of $\langle Y_1^0 \rangle$, $\langle Y_2^0 \rangle$, and σ_T calculated from the phase shift solutions of Fig. 28 with the extrapolated moments and total cross section.

Fig. 30. s-wave phase shift δ_1^0 from a fit like that used for Fig. 28, except with p-wave parameters $M = 900$ and $\Gamma = 50$ MeV.

Fig. 31. Effective range fit to the phase shift of the "down" solution.

Fig. 32. Extrapolated $\langle Y_1^0 \rangle$, $\langle Y_2^0 \rangle$, and σ_T. The curves are the results of energy-dependent fits. The solid curve represents the best fit for the nonresonant hypothesis; the dashed curve is the fit for an s-wave resonance with $\Gamma = 7$ MeV added to an effective-range background.

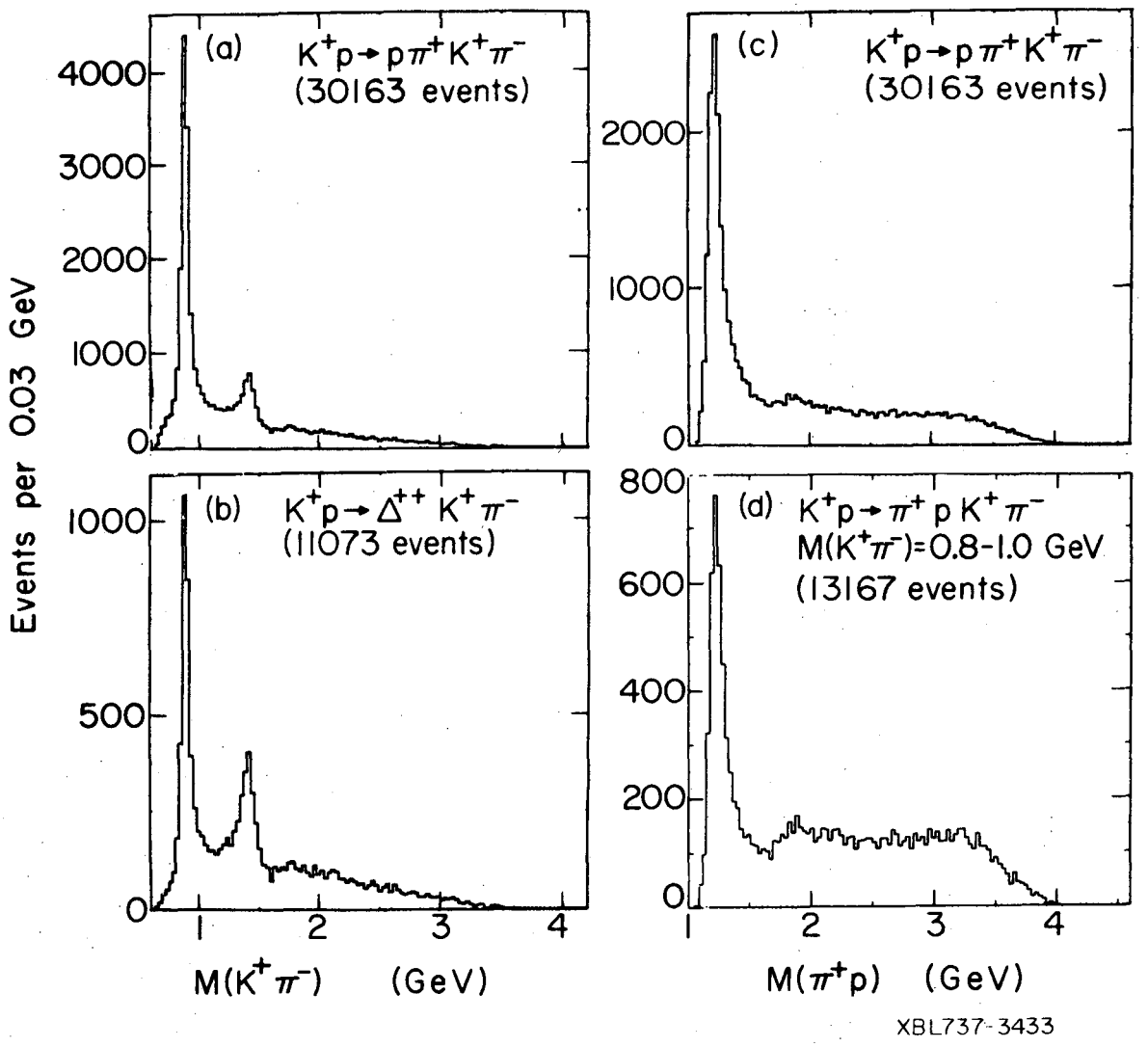
(a)
$K^+p \to p\pi^+K^+\pi^-$
(30163 events)
(b)
$K^+p \to \Delta^{++}K^+\pi^-$
(11073 events)
(c)
$K^+p \to p\pi^+K^+\pi^-$
(30163 events)
(d)
$K^+p \to \pi^+pK^+\pi^-$
$M(K^+\pi^-)$=0.8-1.0 GeV
(13167 events)
Events per 0.03 GeV
$M(K^+\pi^-)$ (GeV)
$M(\pi^+p)$ (GeV)
XBL737-3433

Fig. 1

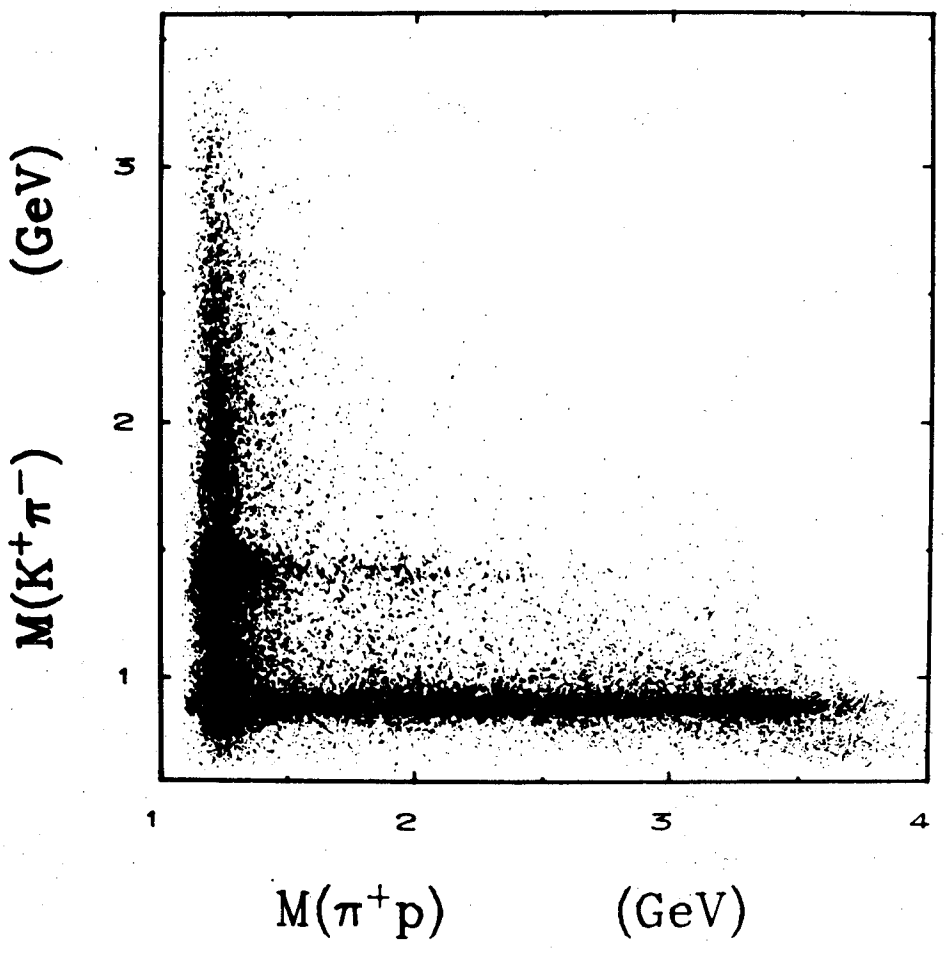

XBL 737-884

Fig. 2

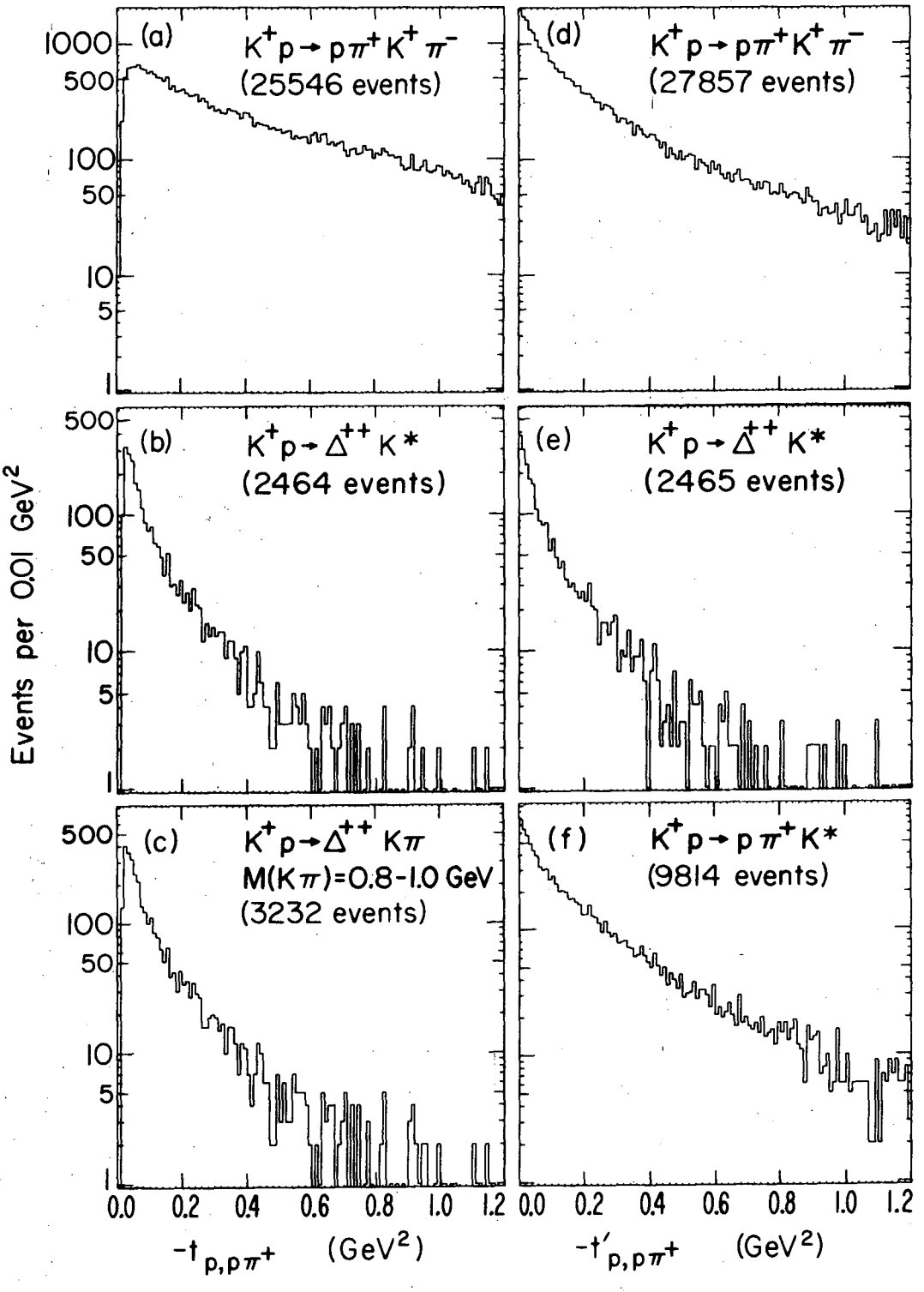
(a)
$K^+p \to p\pi^+K^+\pi^-$
(25546 events)
(d)
$K^+p \to p\pi^+K^+\pi^-$
(27857 events)
(b)
$K^+p \to \Delta^{++}K^*$
(2464 events)
(e)
$K^+p \to \Delta^{++}K^*$
(2465 events)
(c)
$K^+p \to \Delta^{++}K\pi$
$M(K\pi)$=0.8-1.0 GeV
(3232 events)
(f)
$K^+p \to p\pi^+K^*$
(9814 events)
Events per 0.01 GeV^2
$-t_{p,p\pi^+}$ (GeV^2)
$-t'_{p,p\pi^+}$ (GeV^2)
XBL737-3434

Fig. 3

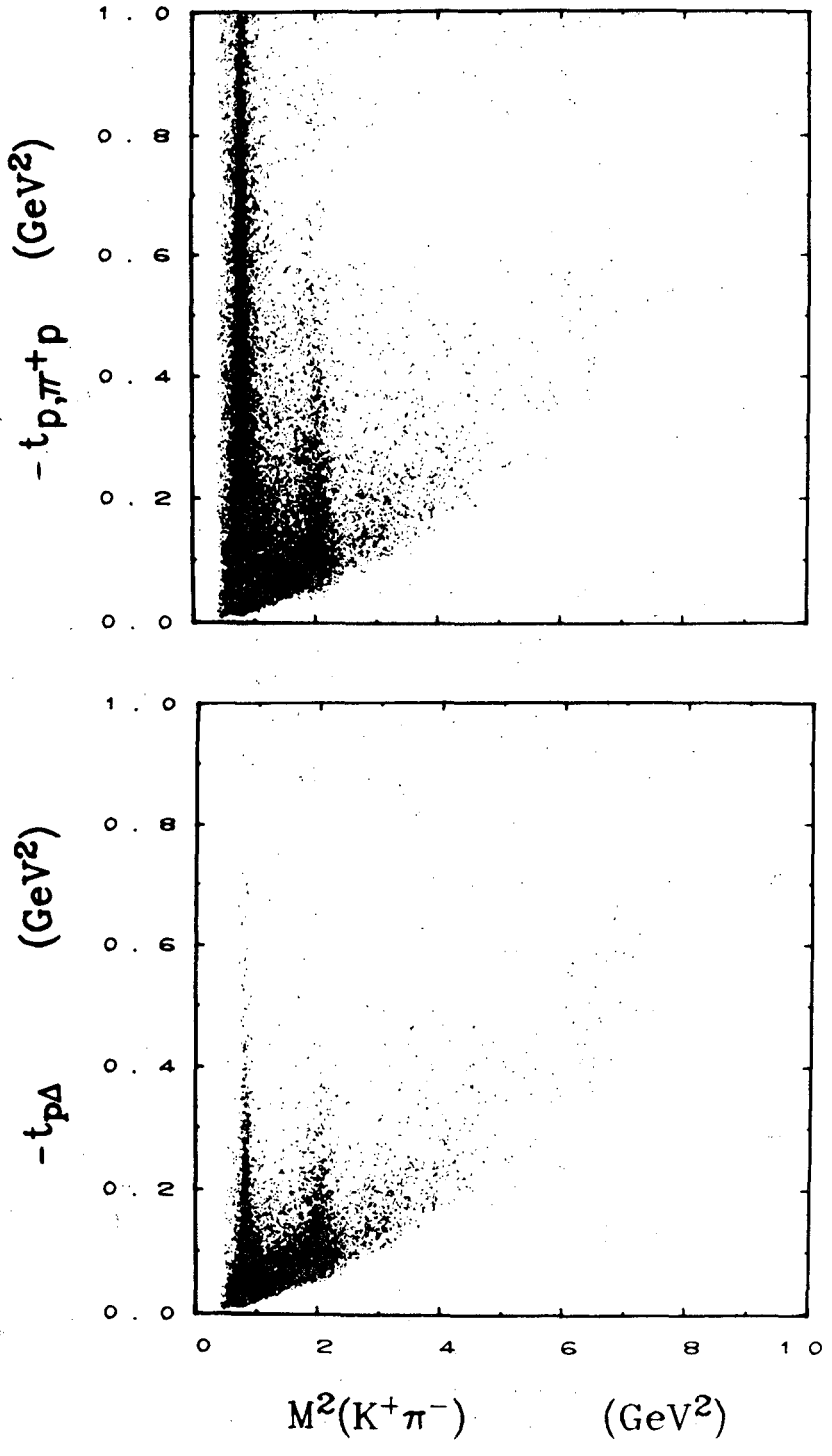

XBL7212-4932

Fig. 4

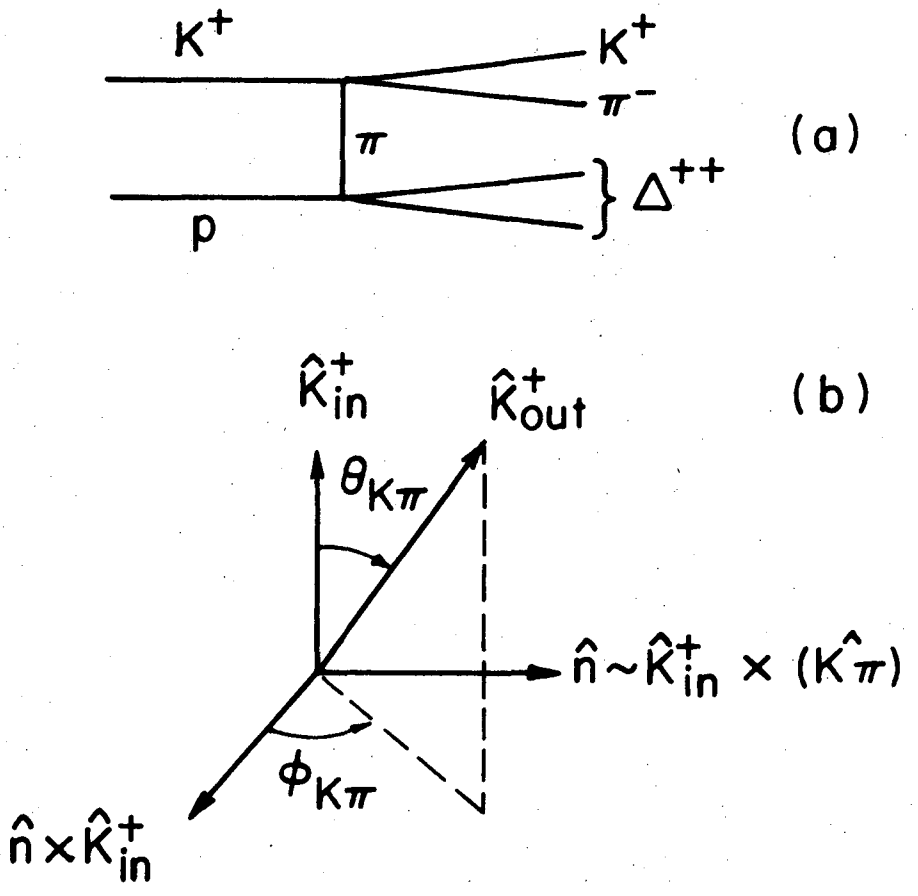

XBL736-3049

Fig. 5

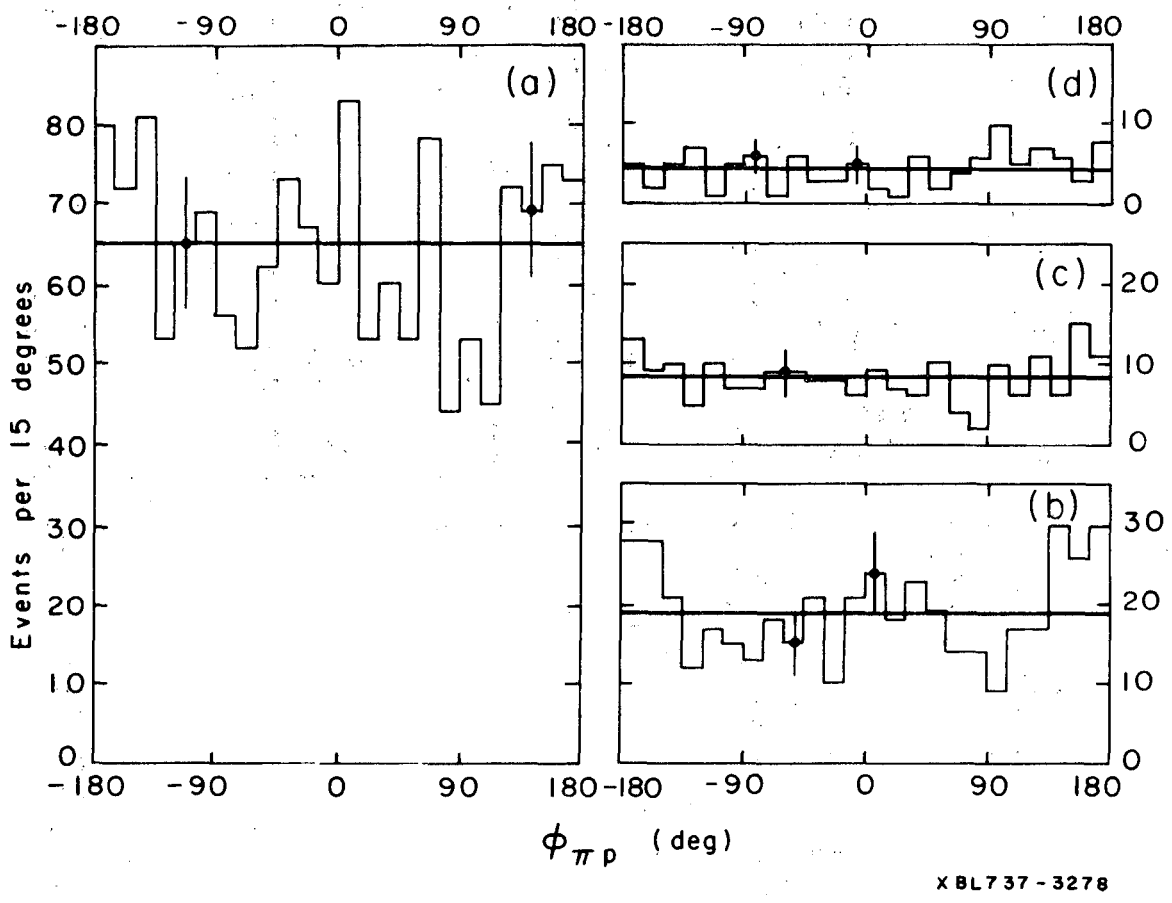

Fig. 6

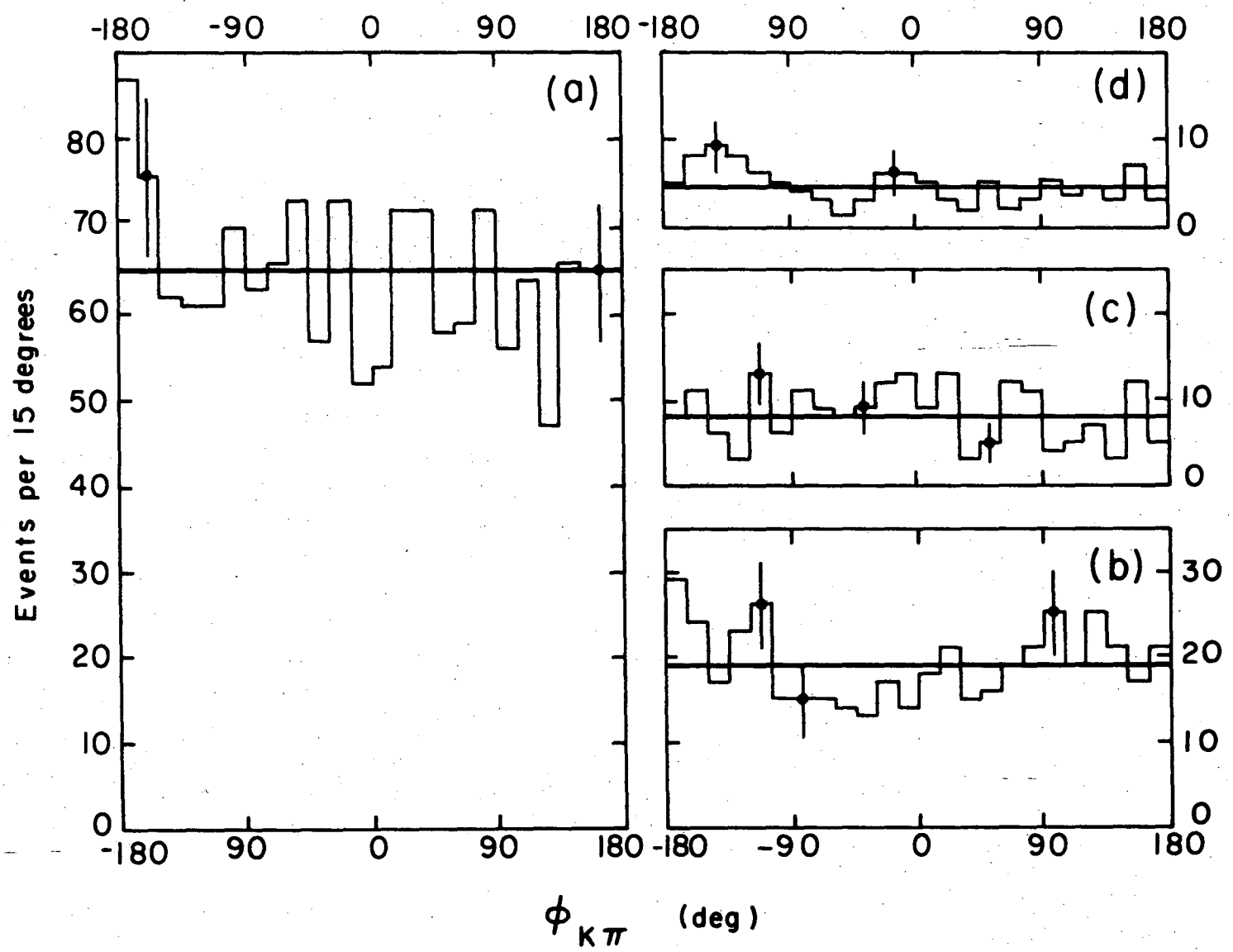

XBL737-3277

Fig. 7

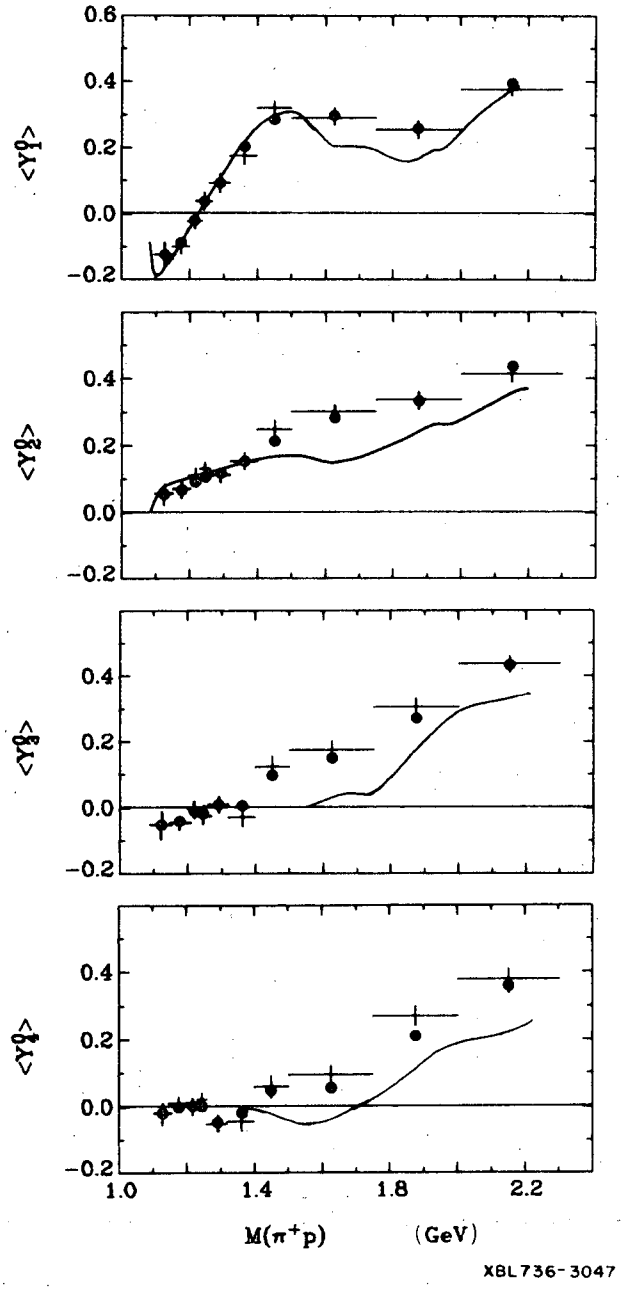

Fig. 8

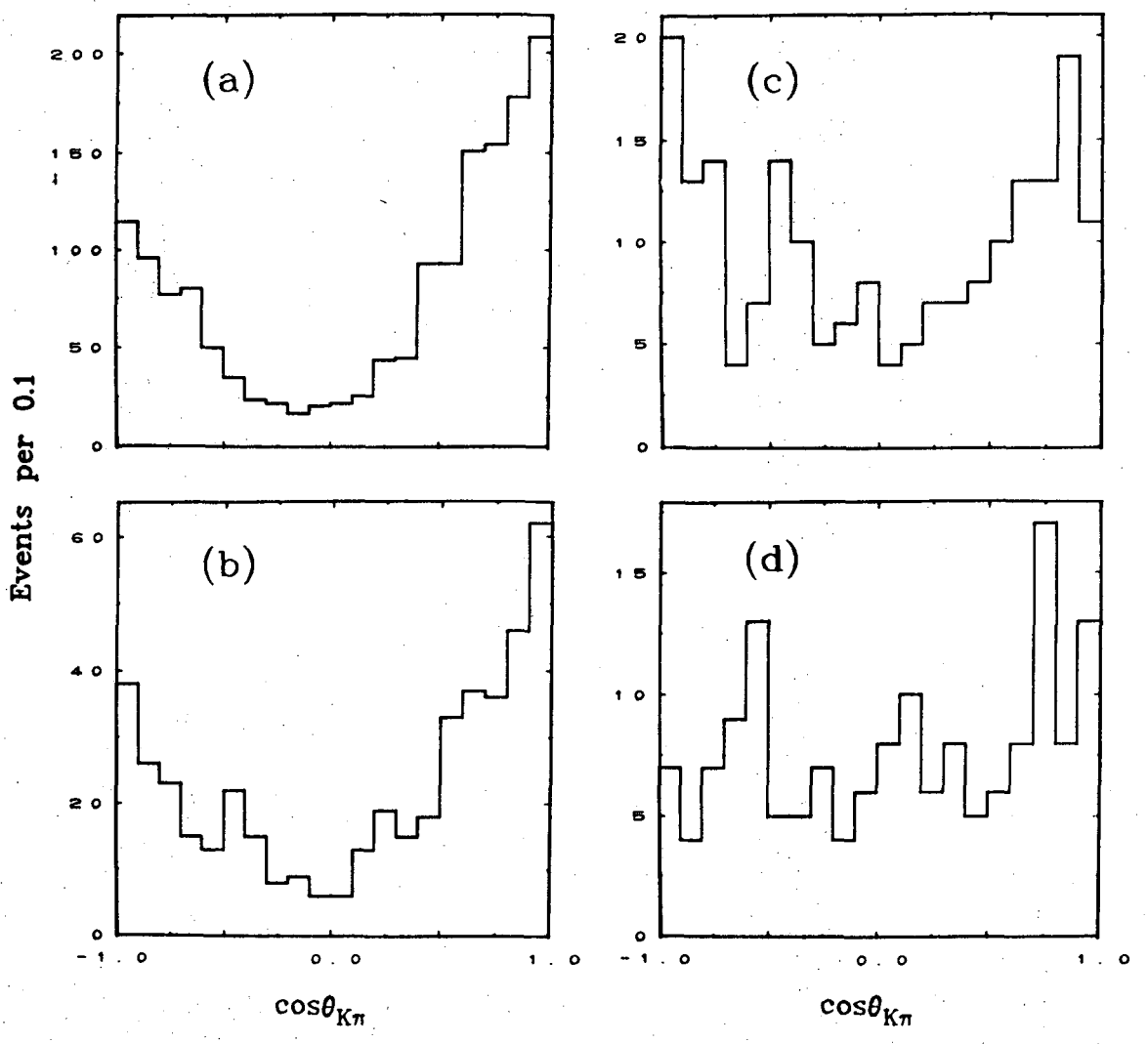

XBL 7212-5661

Fig. 9

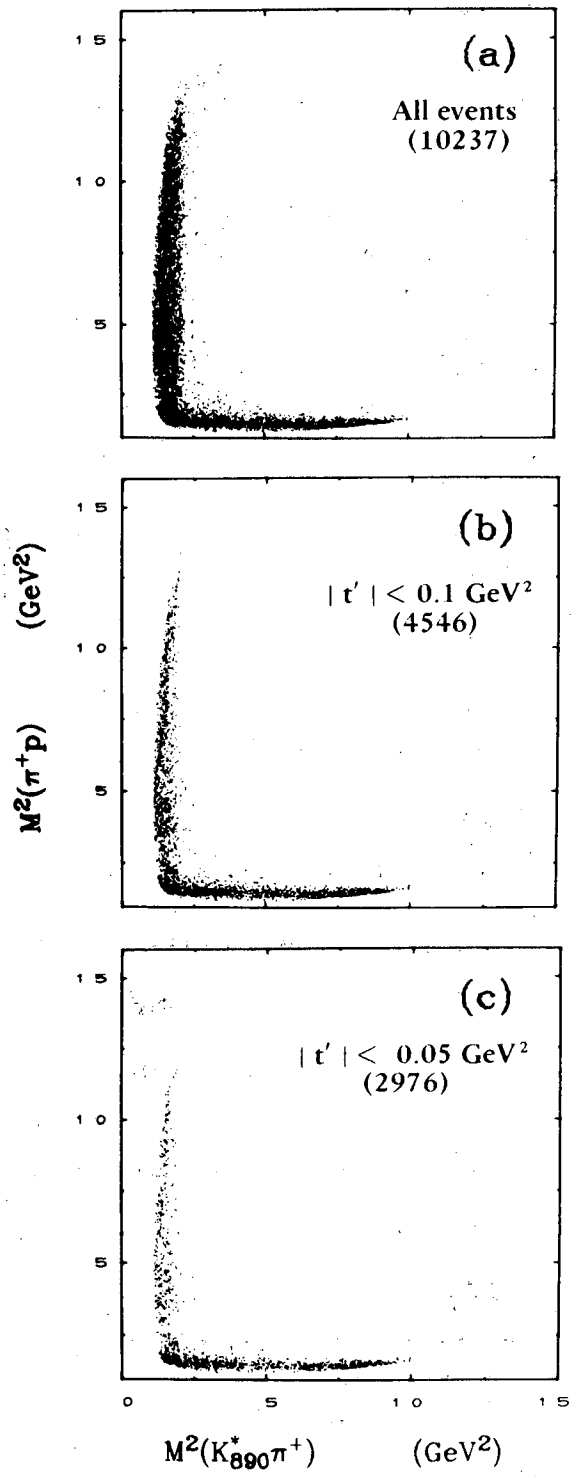

XBL 7212-5663

Fig. 10

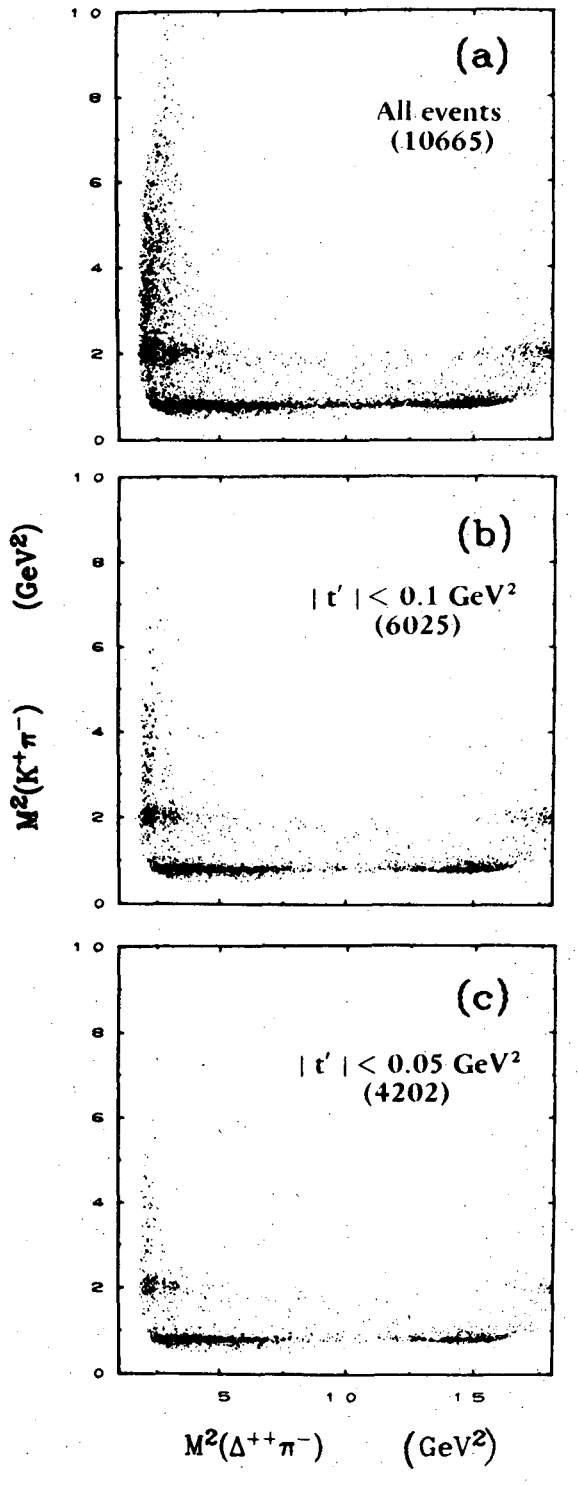

XBL 7212-5670

Fig. 11

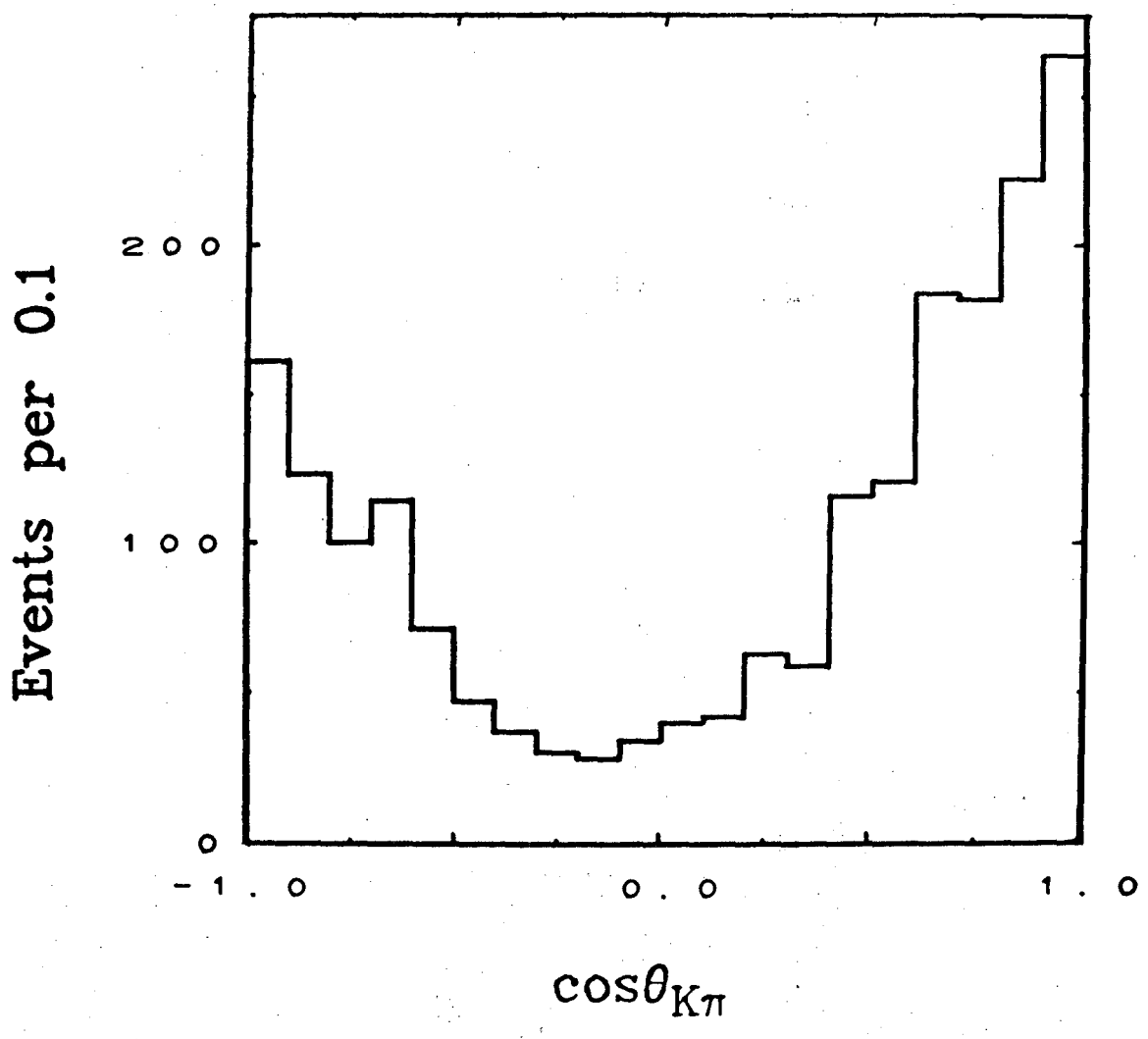

XBL 7212-5666

Fig. 12

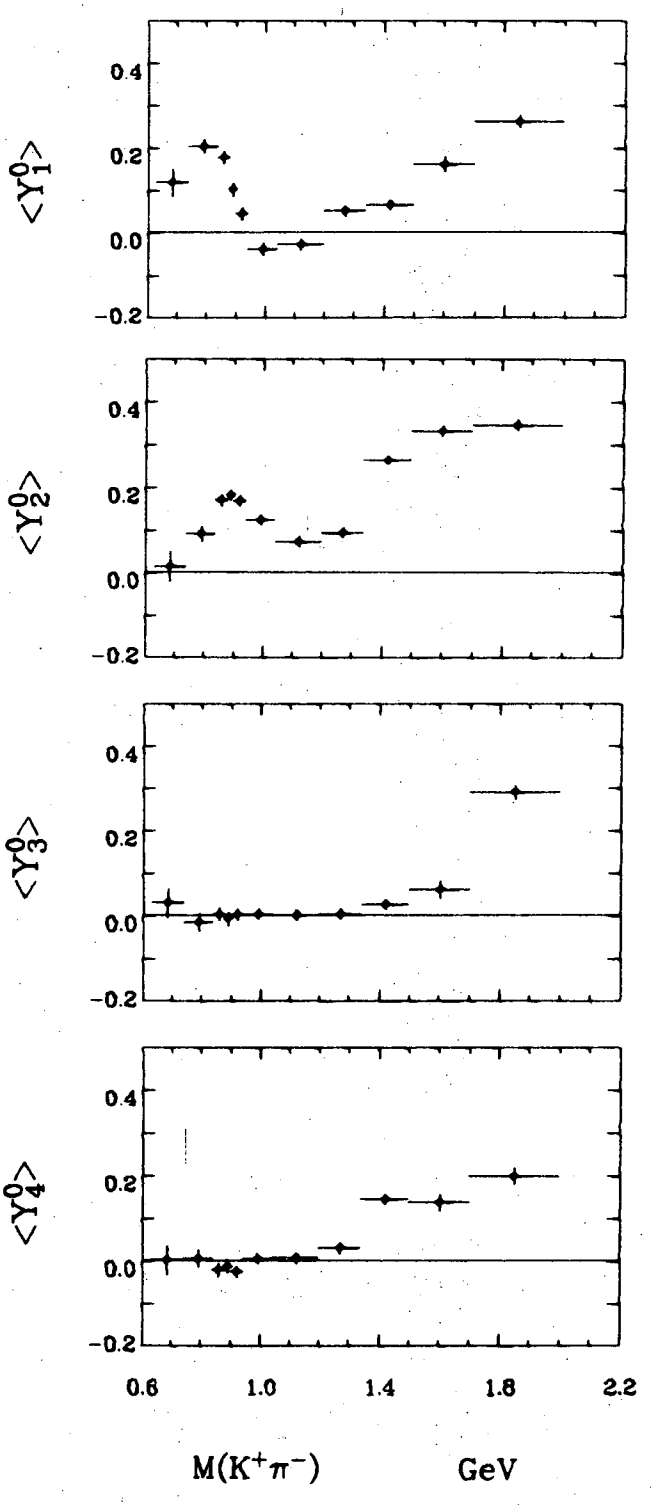

XBL 7212-5657

Fig. 13

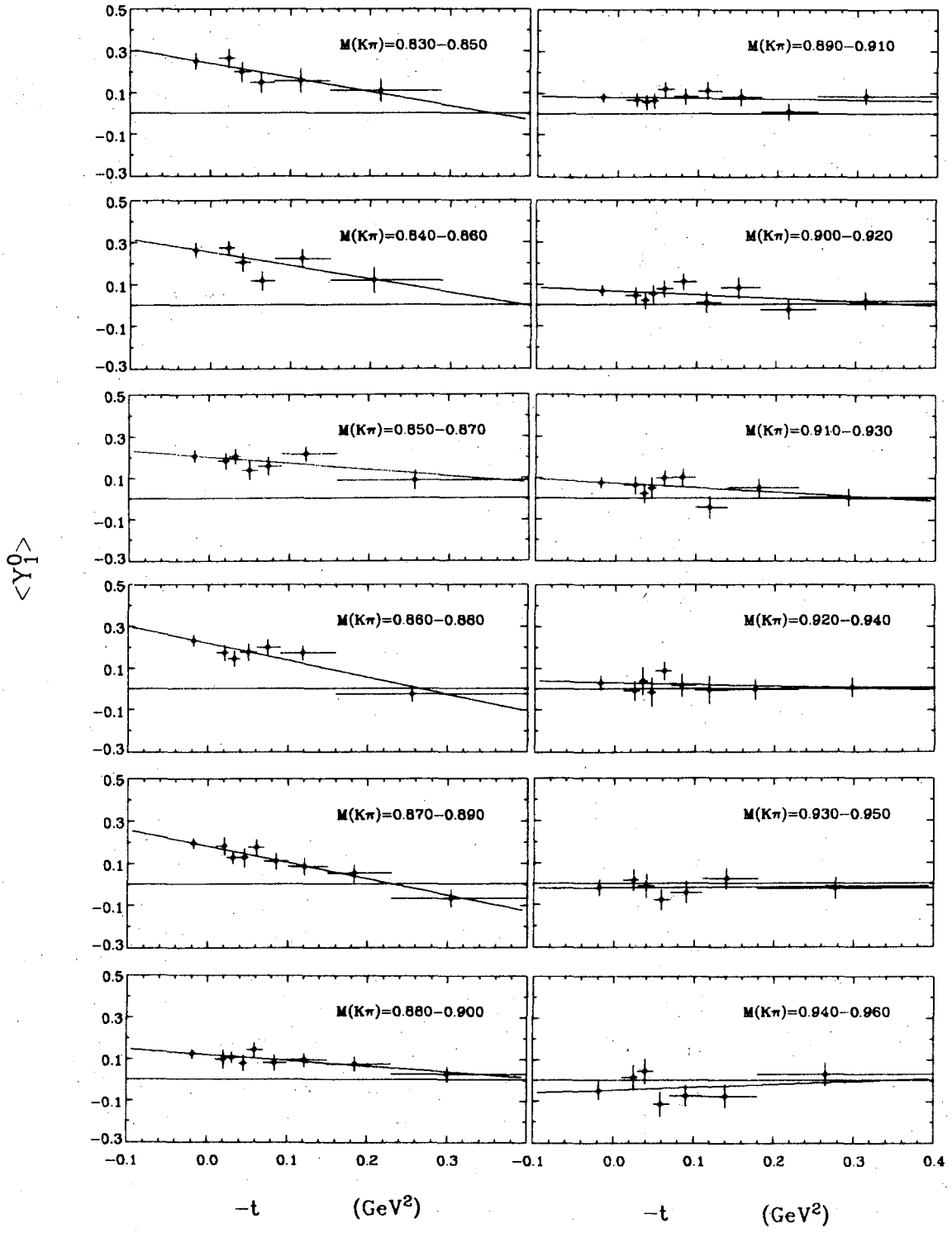

XBL 7212-5665

Fig. 14

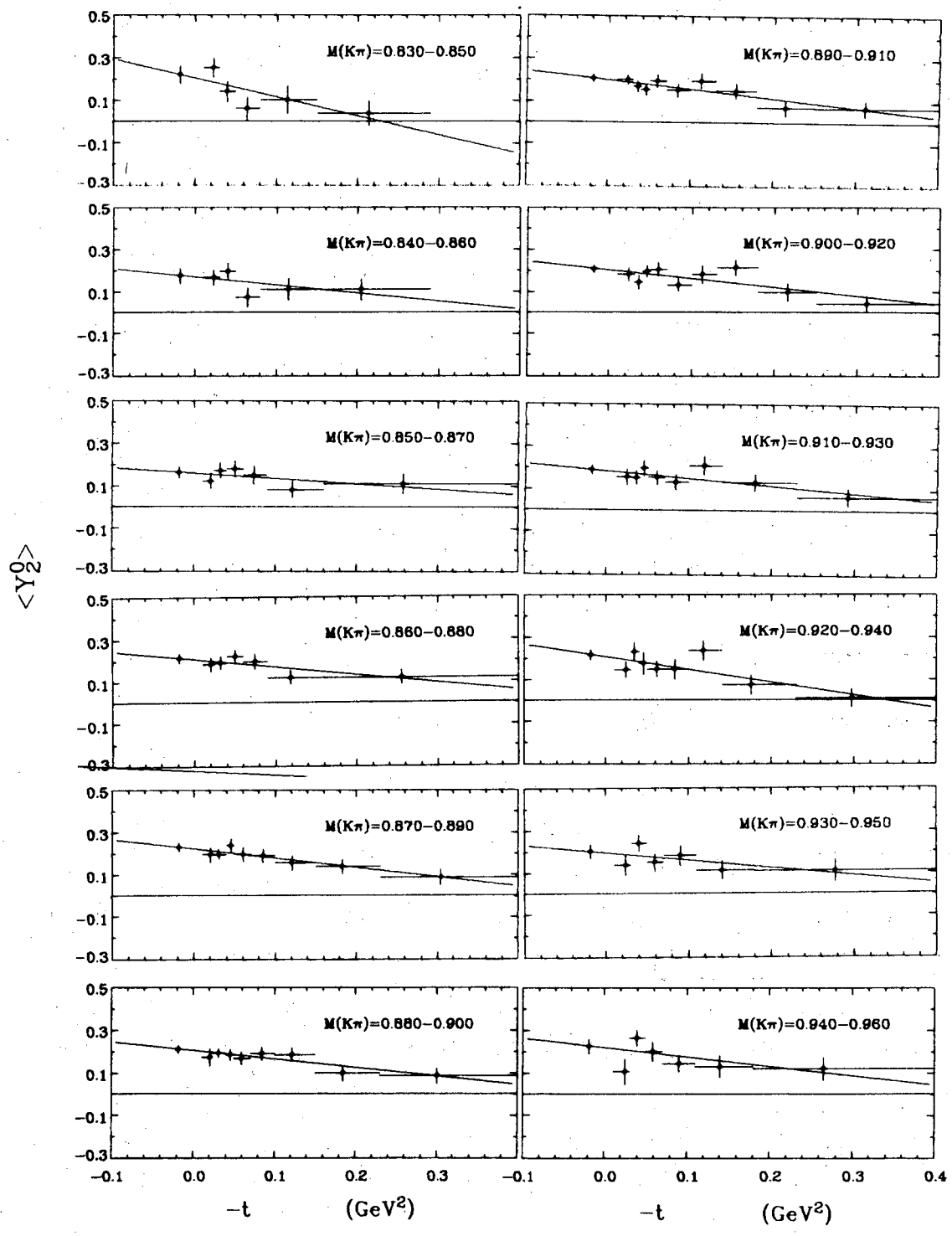

XBL 7212-5662

Fig. 15

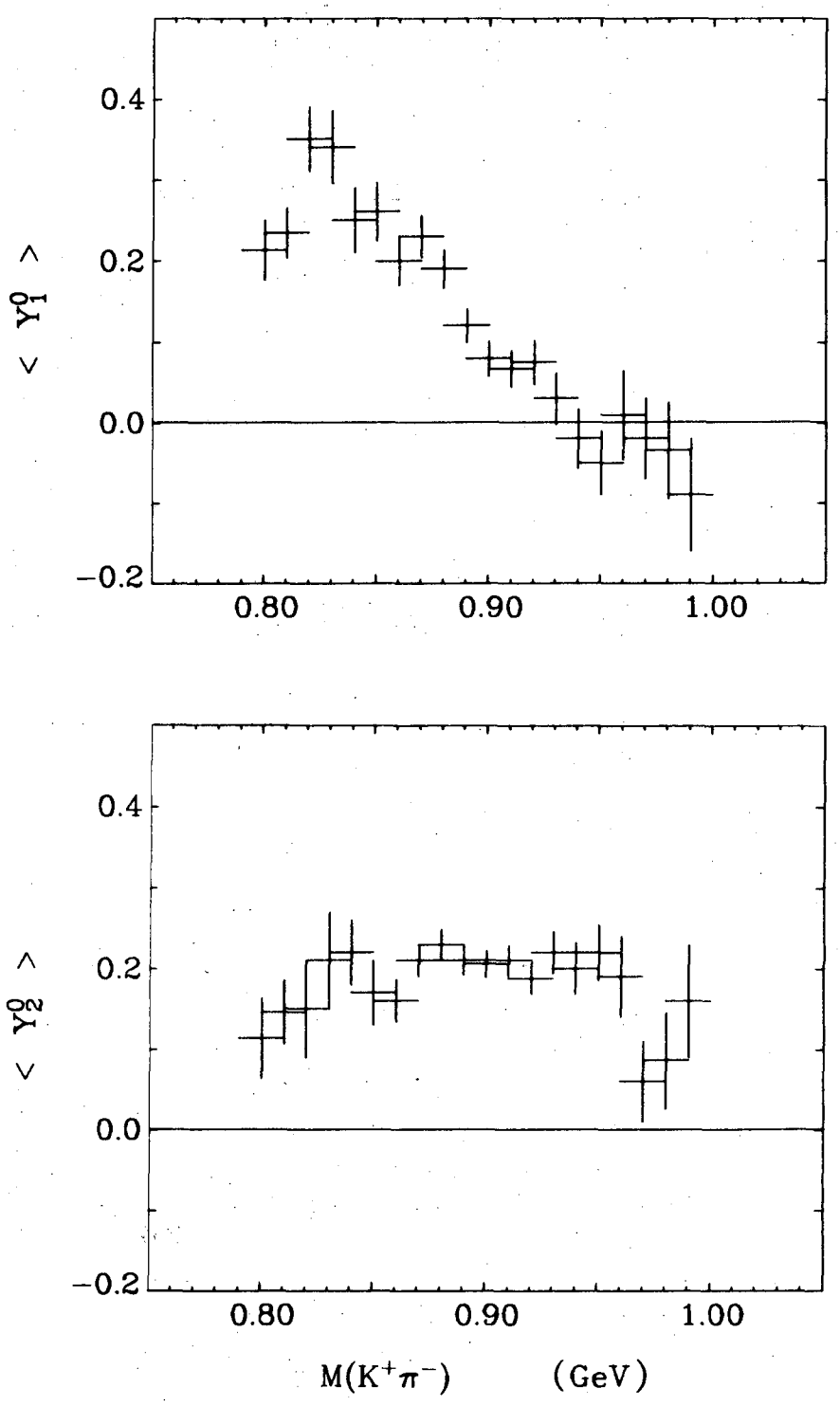

XBL 7212-5650

Fig. 16

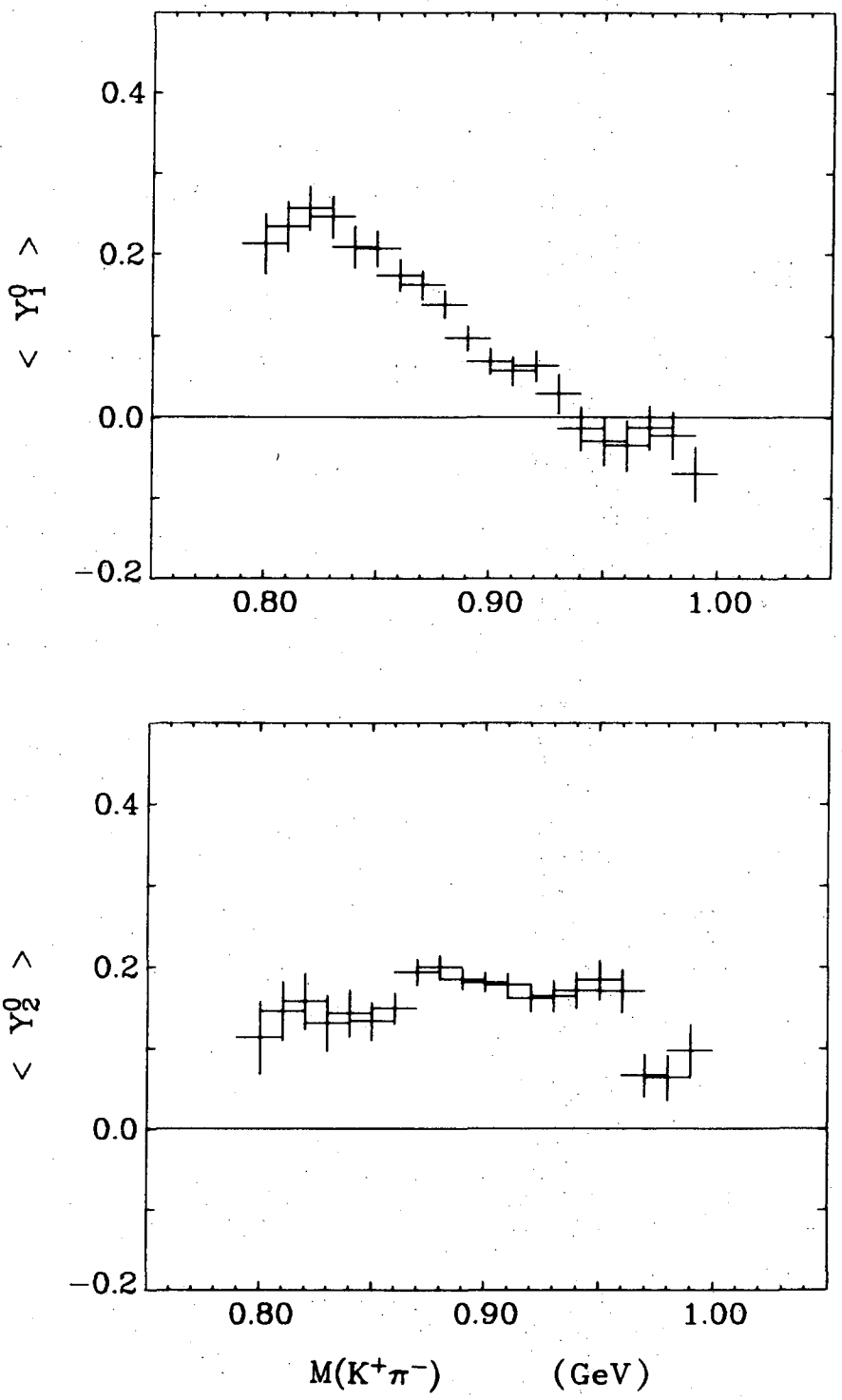

XBL 7212-5651

Fig. 17

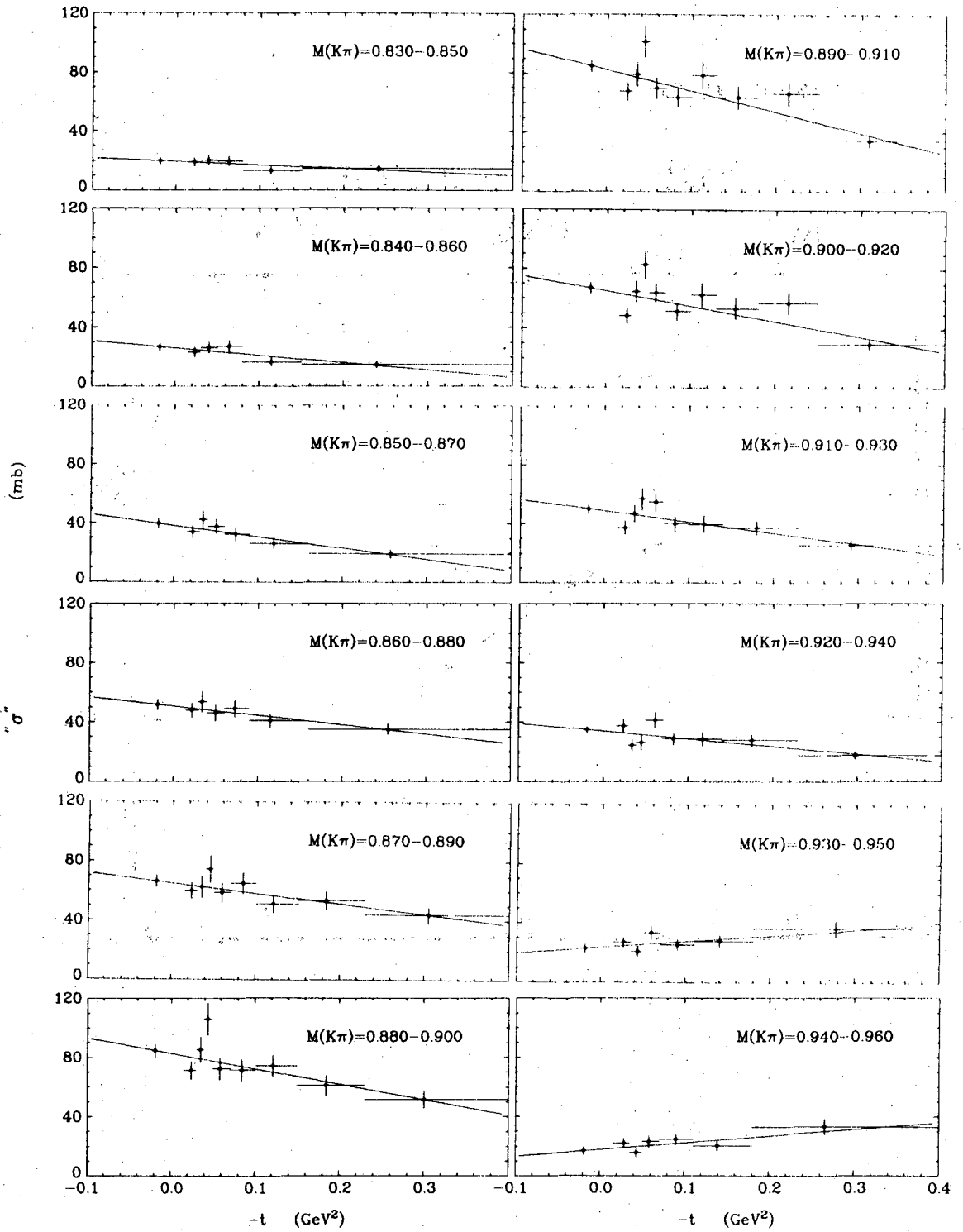
M(Kπ)=0.830–0.850
M(Kπ)=0.840–0.860
M(Kπ)=0.850–0.870
M(Kπ)=0.860–0.880
M(Kπ)=0.870–0.890
M(Kπ)=0.880–0.900
M(Kπ)=0.890–0.910
M(Kπ)=0.900–0.920
M(Kπ)=0.910–0.930
M(Kπ)=0.920–0.940
M(Kπ)=0.930–0.950
M(Kπ)=0.940–0.960
"σ" (mb)
120
80
40
0
−0.1
0.0
0.1
0.2
0.3
0.4
−t (GeV²)

Fig. 18

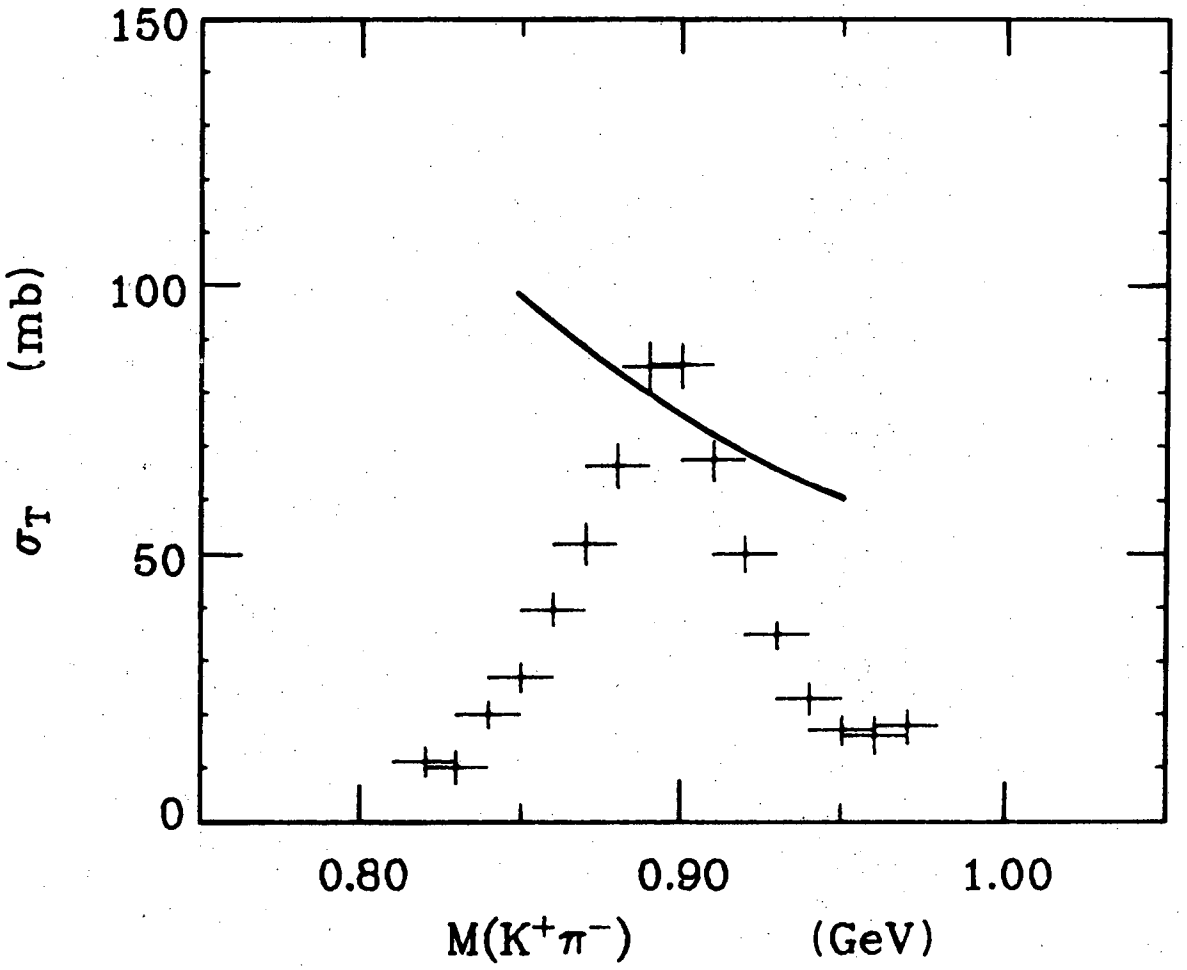

XBL7212-4920

Fig. 19

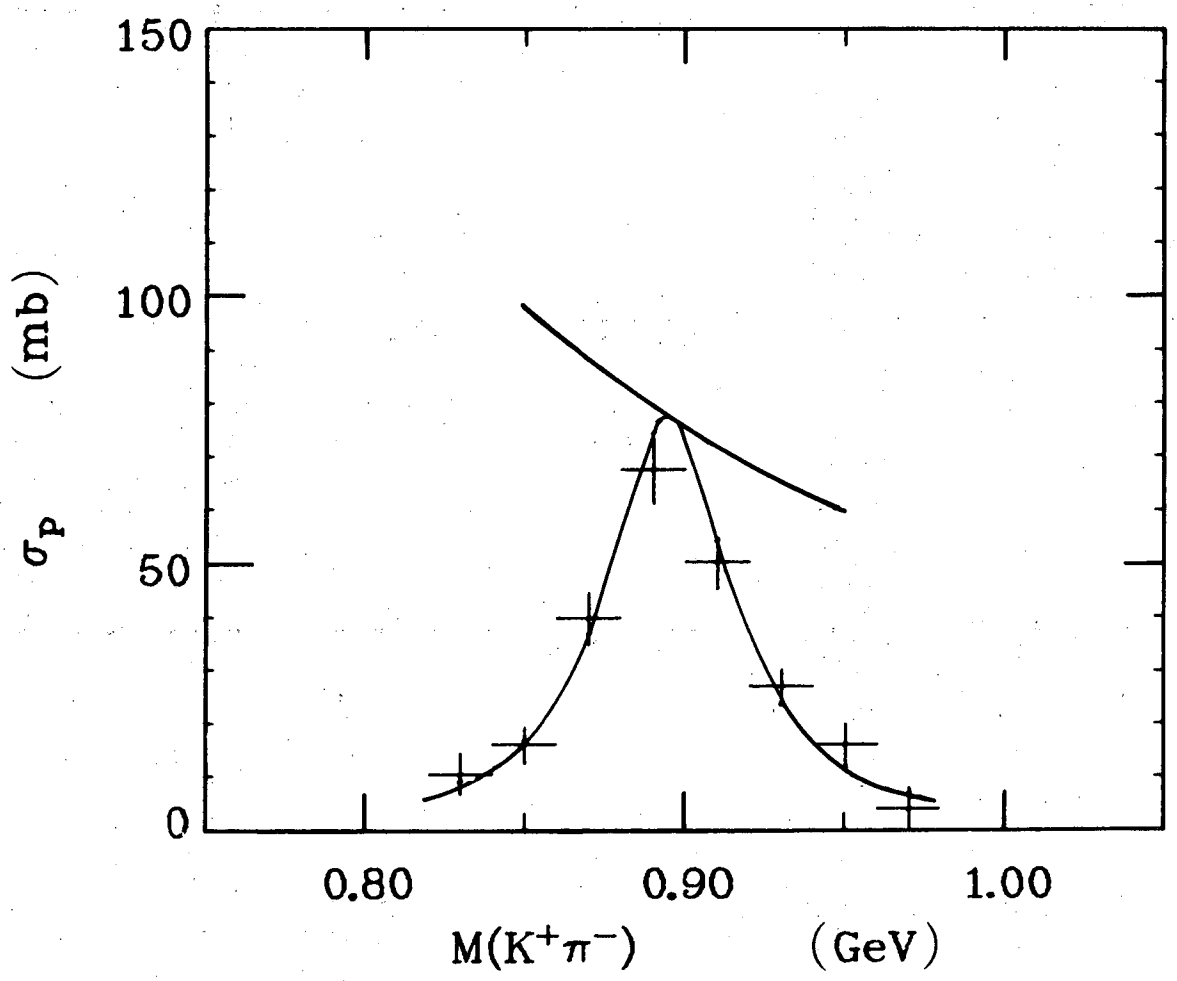

XBL 7212-4918

Fig. 20

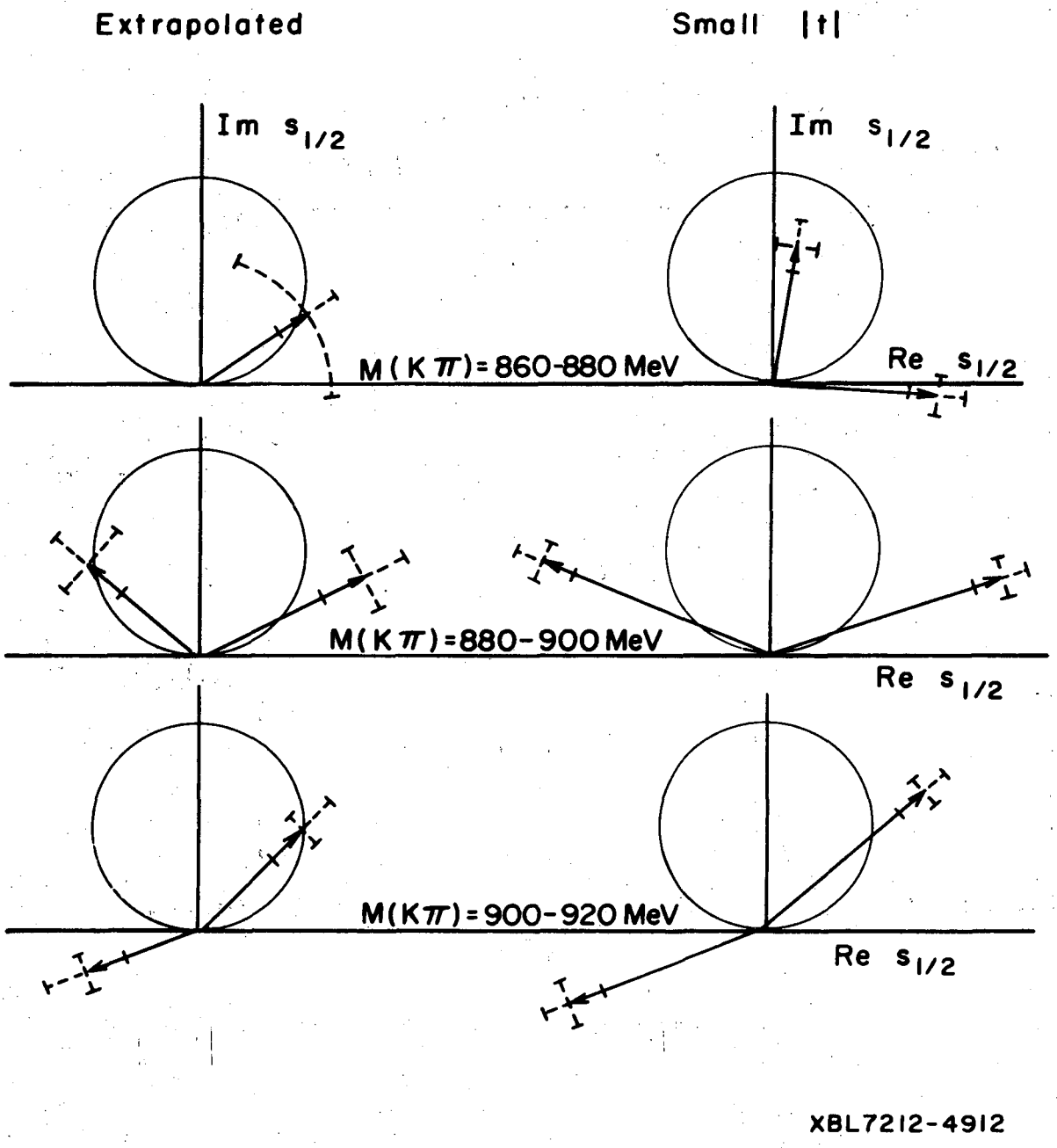
Extrapolated
Small |t|
Im $s_{1/2}$
Im $s_{1/2}$
M(Kπ)=860-880 MeV
Re $s_{1/2}$
M(Kπ)=880-900 MeV
Re $s_{1/2}$
M(Kπ)=900-920 MeV
Re $s_{1/2}$
XBL7212-4912

Fig. 21

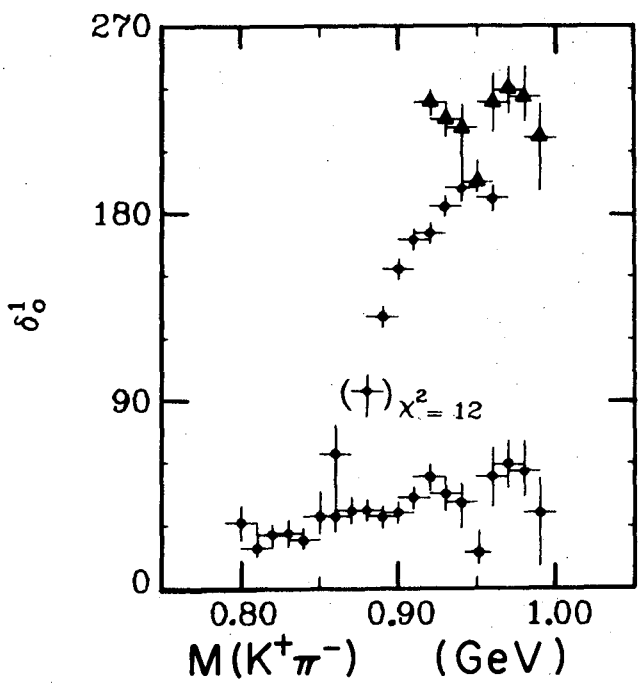

XBL737-3444

Fig. 22

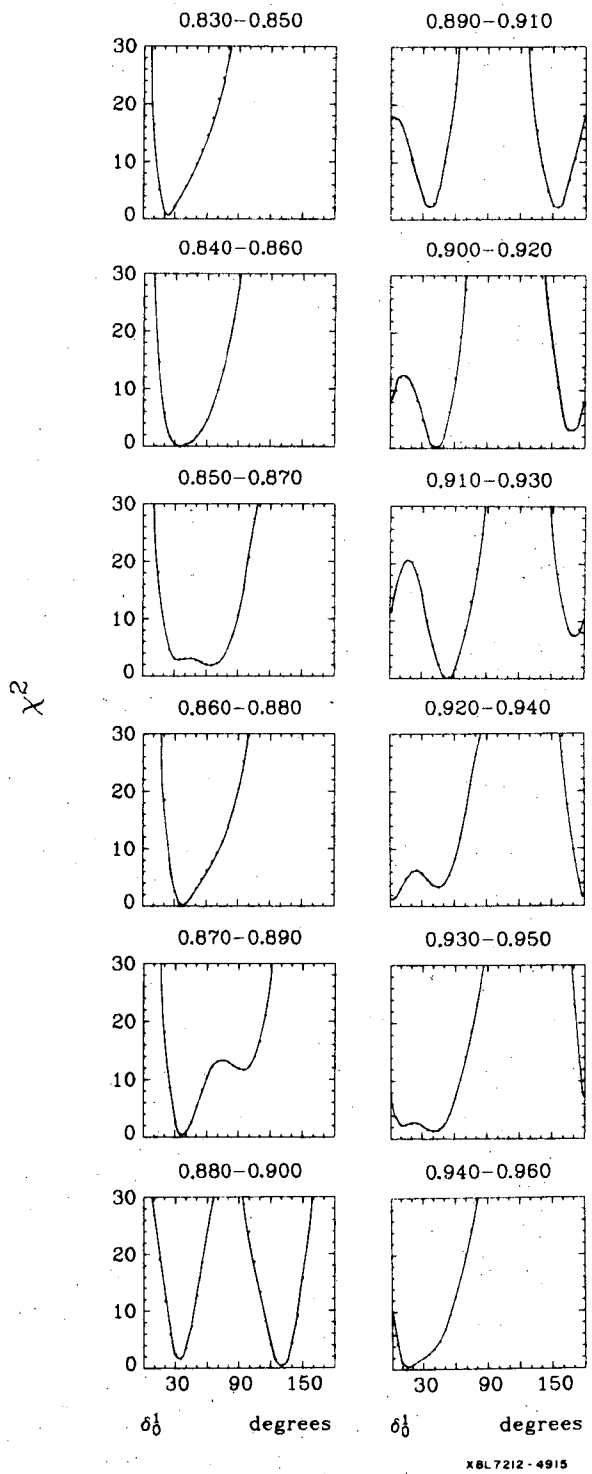
0.830–0.850
0.890–0.910
0.840–0.860
0.900–0.920
0.850–0.870
0.910–0.930
0.860–0.880
0.920–0.940
0.870–0.890
0.930–0.950
0.880–0.900
0.940–0.960
30
20
10
0
30 90 150
δ_0^1 degrees
χ^2
XBL7212-4915

Fig. 23

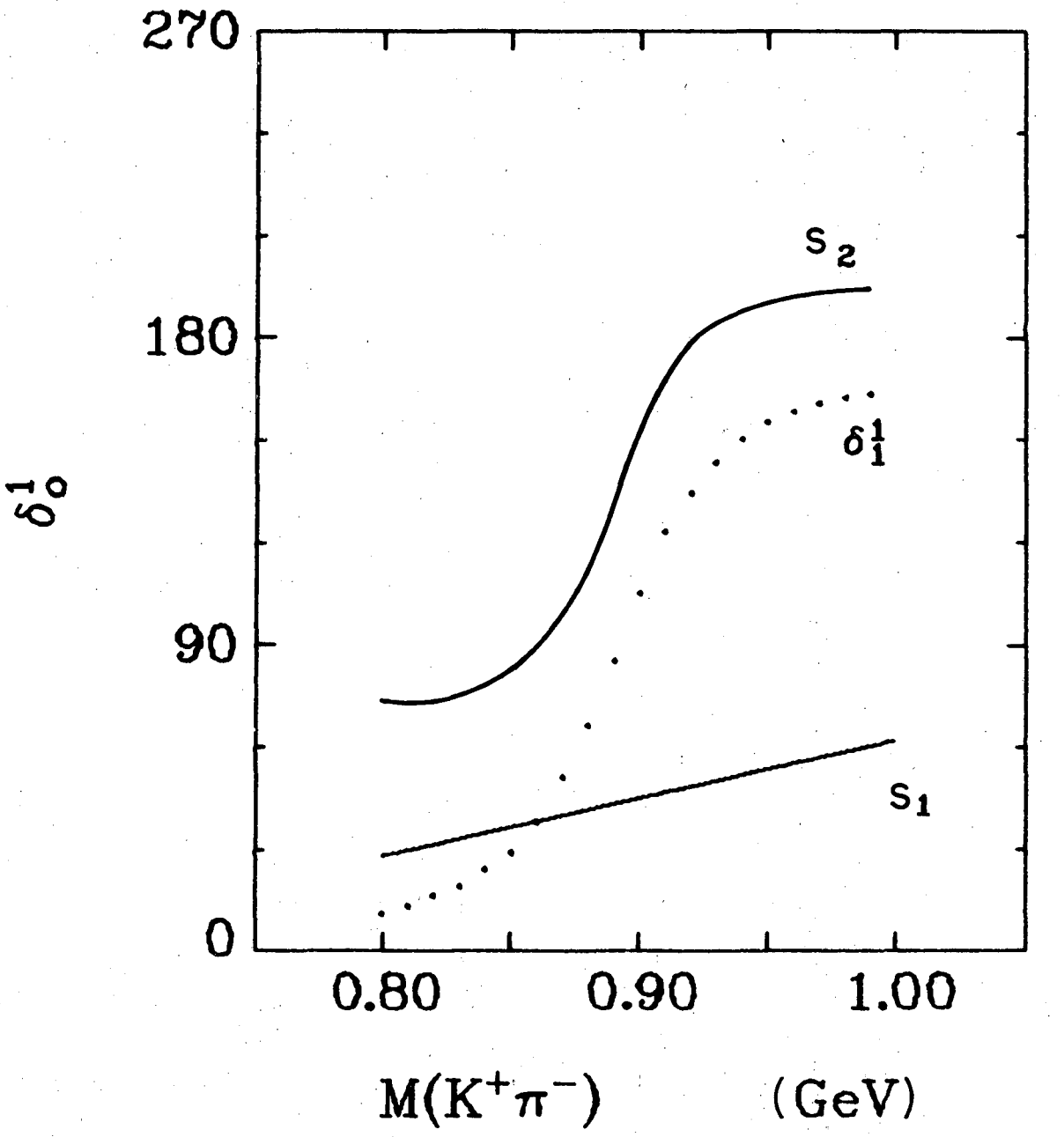

XBL7212-4917

Fig. 24

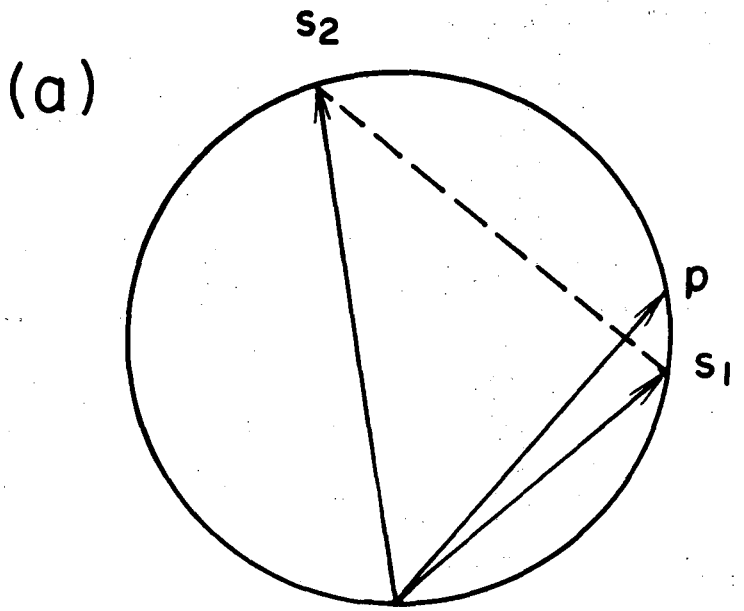

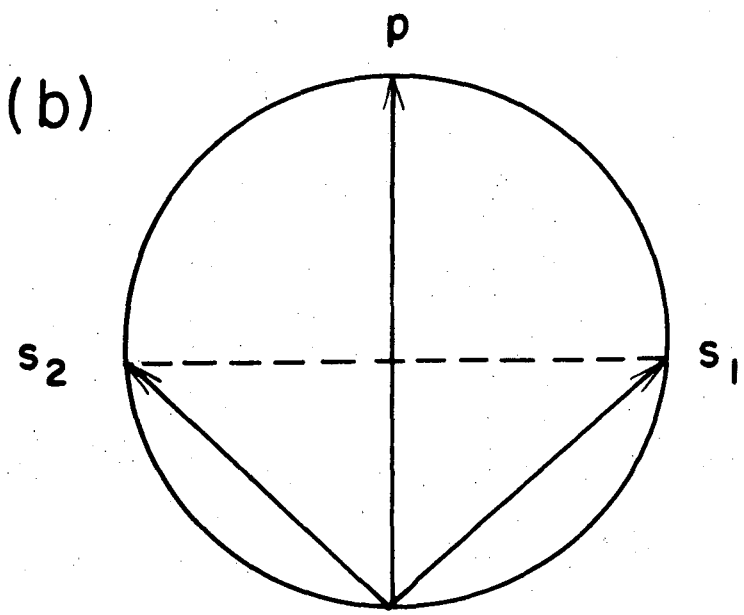

XBL7212-4913

Fig. 25

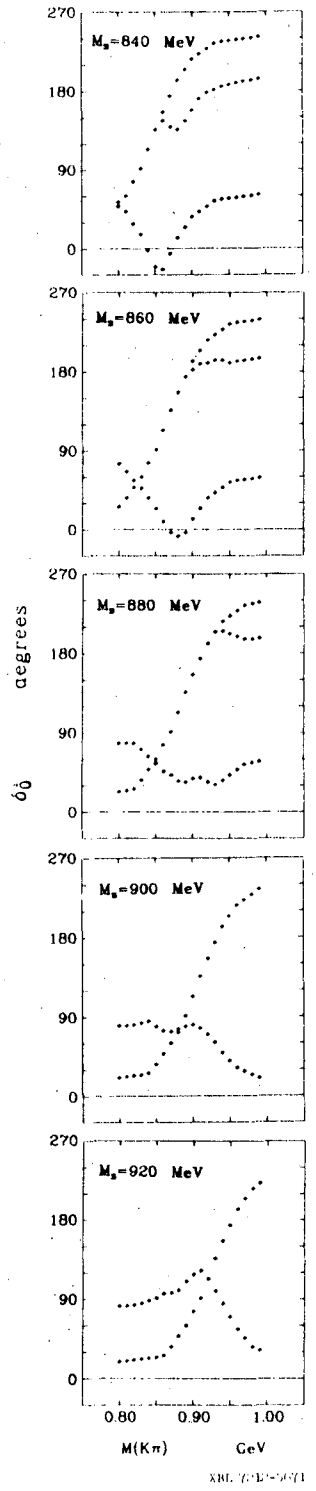
M_s=840 MeV
M_s=860 MeV
M_s=880 MeV
M_s=900 MeV
M_s=920 MeV
270
180
90
0
δ_0 degrees
0.80
0.90
1.00
M(Kπ)
GeV

Fig. 26

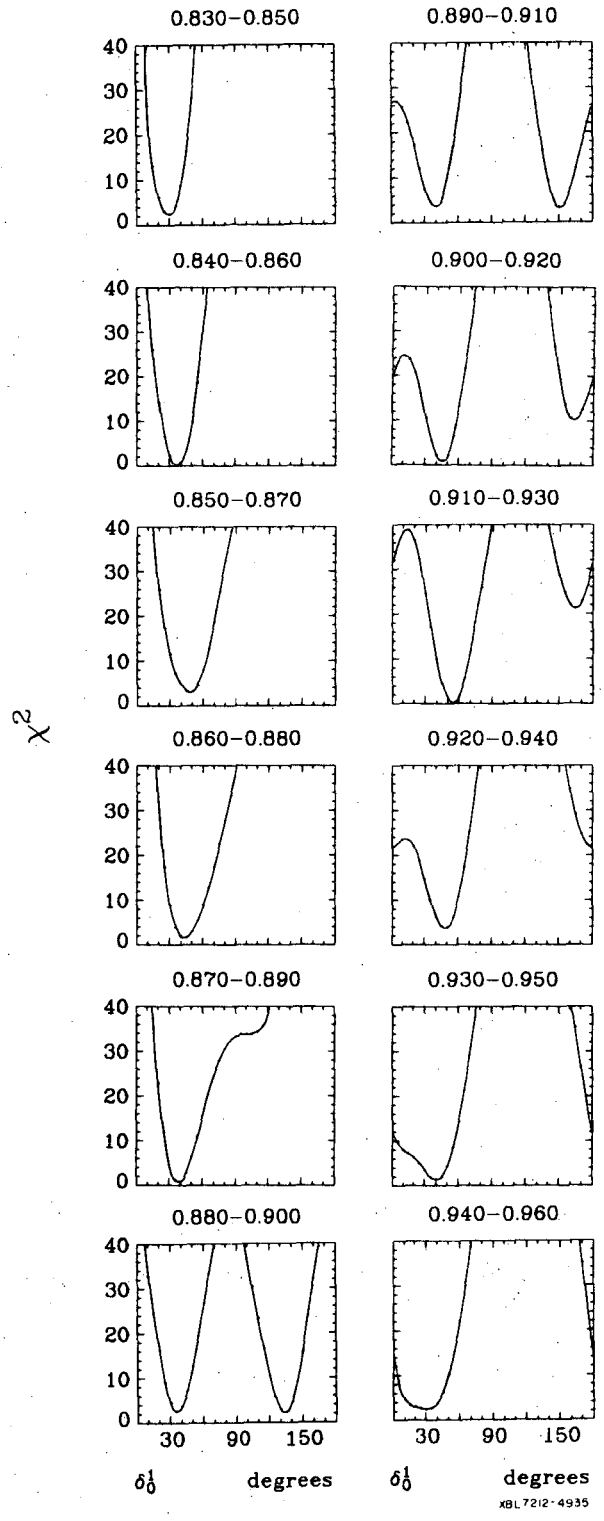
0.830–0.850
0.840–0.860
0.850–0.870
0.860–0.880
0.870–0.890
0.880–0.900
0.890–0.910
0.900–0.920
0.910–0.930
0.920–0.940
0.930–0.950
0.940–0.960
χ^2
40
30
20
10
0
30
90
150
δ_0^1
degrees
XBL7212-4935

Fig. 27

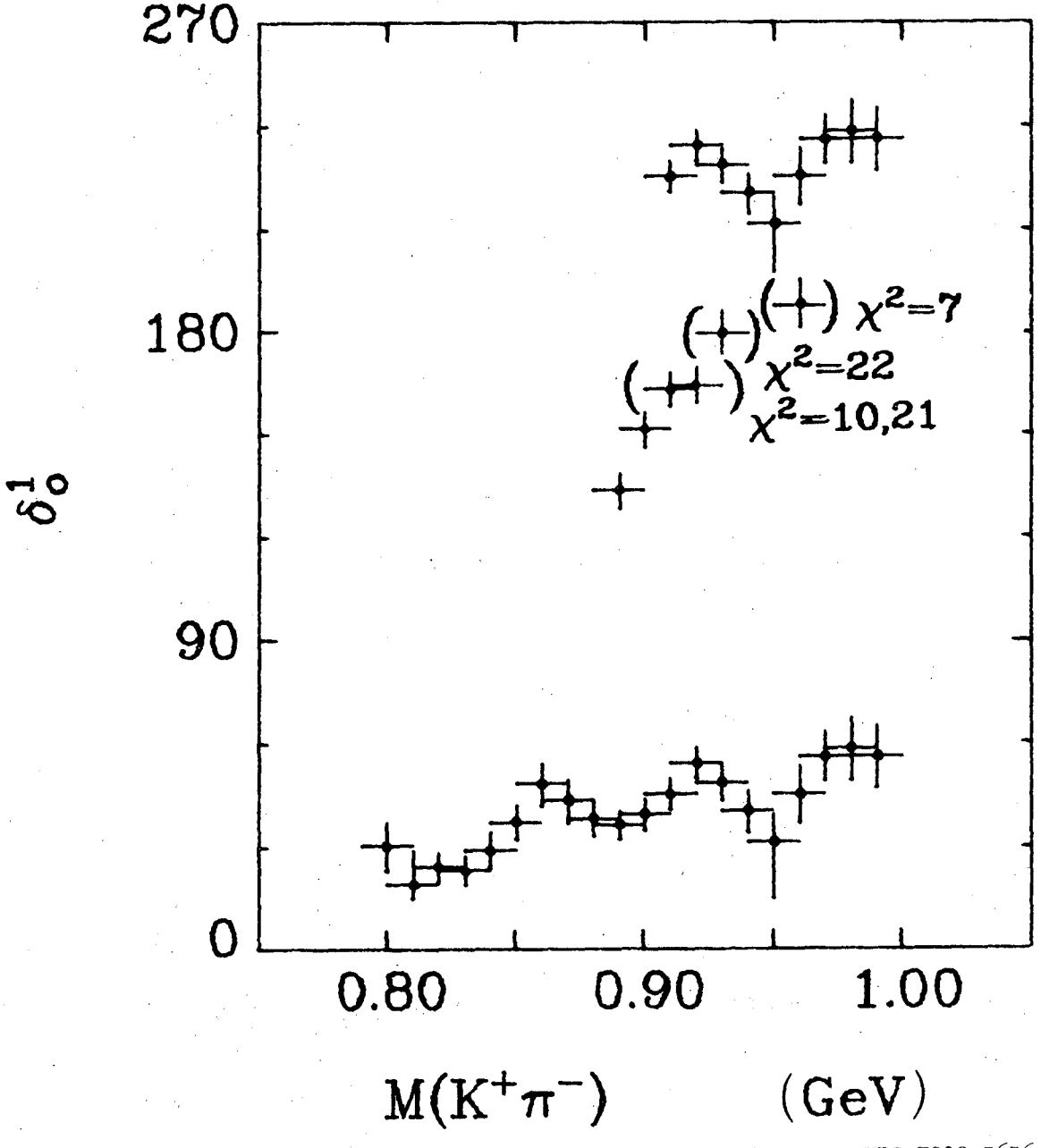

XBL 7212-5656

Fig. 28

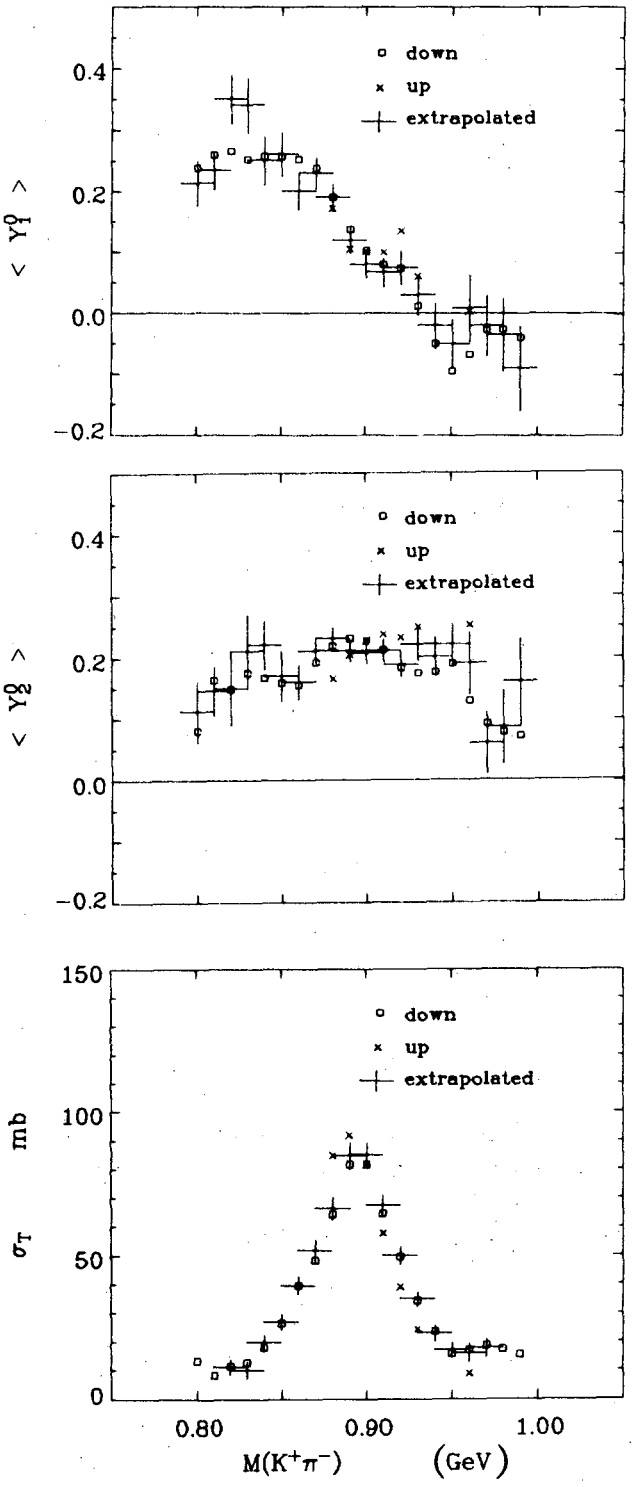

XBL 7212-5653

Fig. 29

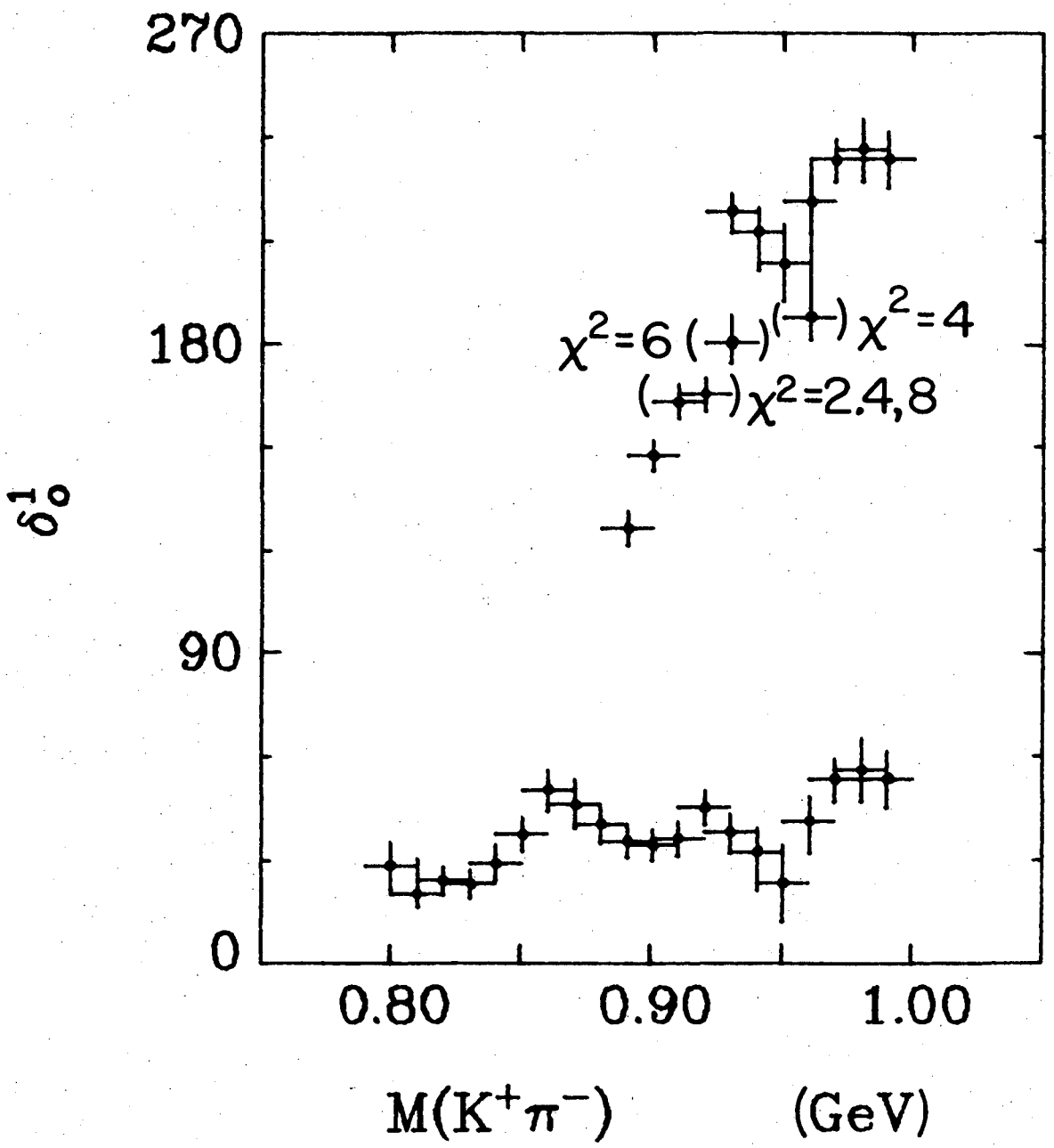

XBL 7212-5655

Fig. 30

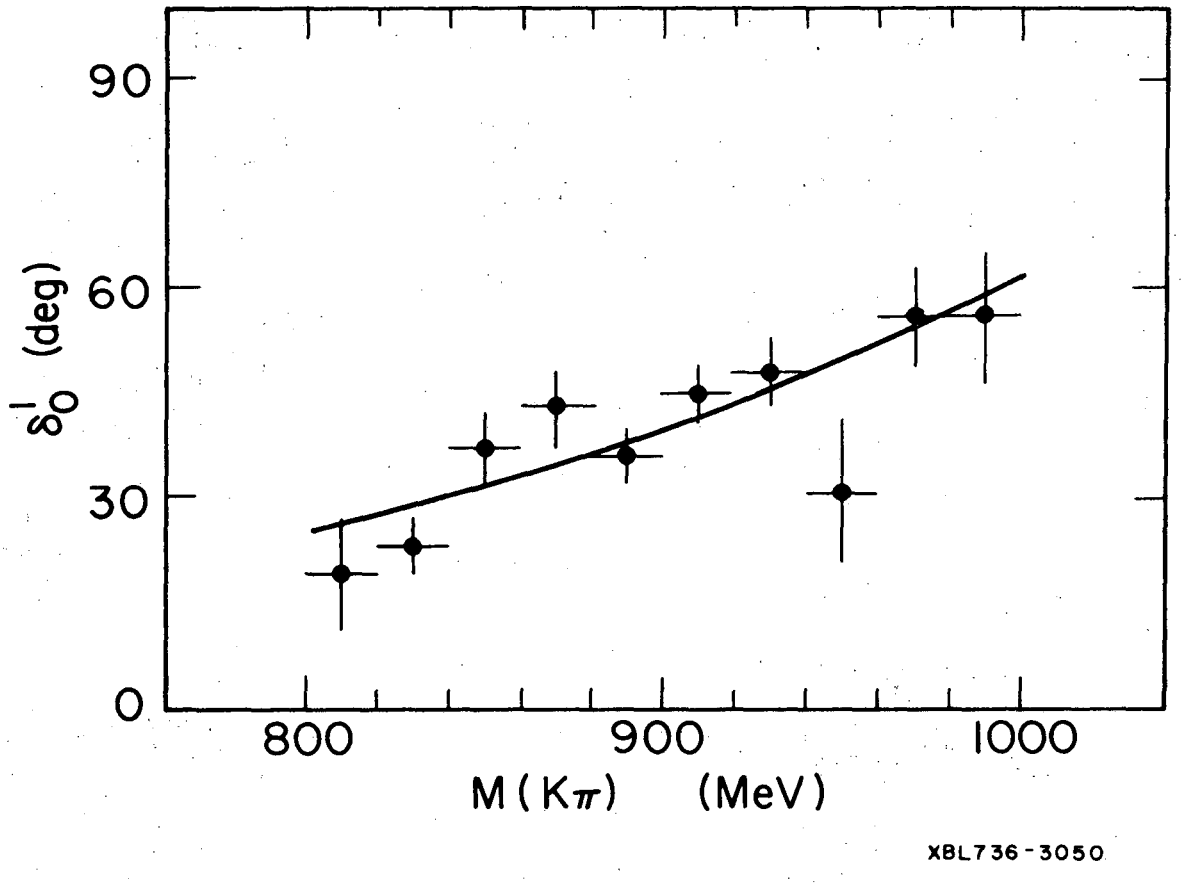

Fig. 31

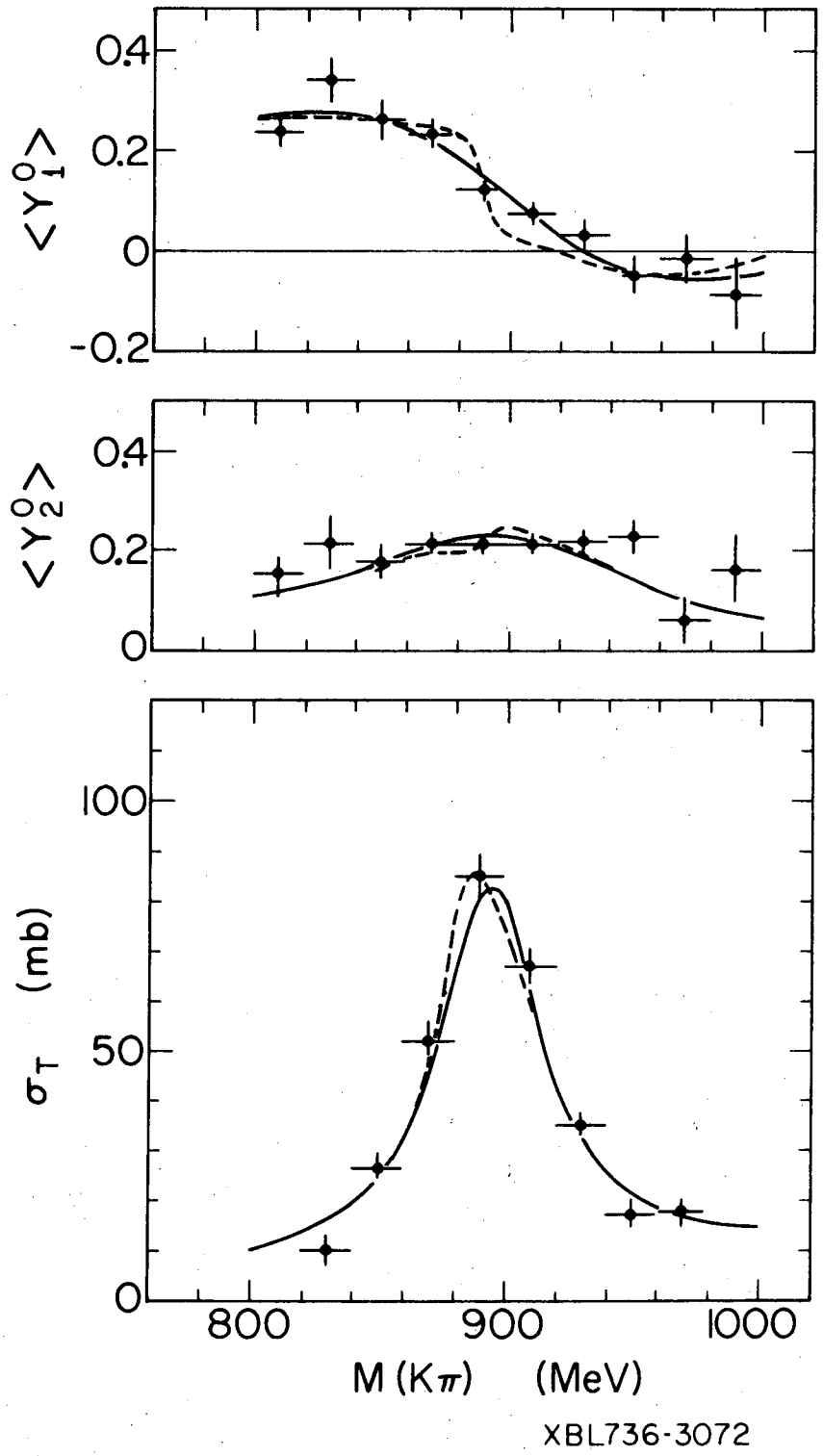
0.4
0.2
0
-0.2
$\langle Y_1^0 \rangle$
0.4
0.2
0
$\langle Y_2^0 \rangle$
100
50
0
σ_T (mb)
800
900
1000
M (Kπ) (MeV)
XBL736-3072

Fig. 32

LEGAL NOTICE

This report was prepared as an account of work sponsored by the United States Government. Neither the United States nor the United States Atomic Energy Commission, nor any of their employees, nor any of their contractors, subcontractors, or their employees, makes any warranty, express or implied, or assumes any legal liability or responsibility for the accuracy, completeness or usefulness of any information, apparatus, product or process disclosed, or represents that its use would not infringe privately owned rights.

TECHNICAL INFORMATION DIVISION
LAWRENCE BERKELEY LABORATORY
UNIVERSITY OF CALIFORNIA
BERKELEY, CALIFORNIA 94720